Energy transfer as a function of collision energy. IV. Statetostate cross sections for rotationaltotranslational energy transfer in HF+Ne, Ar, and Kr

J. A. Barnes, M. Keil, R. E. Kutina, and J. C. Polanyi

Citation: The Journal of Chemical Physics **76**, 913 (1982); doi: 10.1063/1.443062
View online: http://dx.doi.org/10.1063/1.443062
View Table of Contents: http://scitation.aip.org/content/aip/journal/jcp/76/2?ver=pdfcov
Published by the AIP Publishing

Energy transfer as a function of collision energy. IV. State-to-state cross sections for rotational-to-translational energy transfer in HF+Ne, Ar, and Kr

J. A. Barnes, M. Keil, R. E. Kutina,[a] and J. C. Polanyi

Department of Chemistry, University of Toronto, Toronto, Ontario, M5S 1A1 Canada
(Received 9 September 1981; accepted 22 September 1981)

State-to-state cross sections for rotationally inelastic collisions of HF (v,J) with Ne, Ar, and Kr have been measured. Laser pumping of the molecular beam to the initial states $v=1$, $J=1$–6, and $v=2$, $J=2$, followed by infrared fluorescence, permitted measurements of relative cross sections with $|\Delta J| \lesssim 8$. The collision energy was varied between 4 and 16 kcal/mol. These cross sections could be fitted well using an inverse-power dependence on the rotational energy gap [due to Pritchard and co-workers; J. Chem. Phys. 70, 4155 (1979)] for rotational energy transfers of up to 55% of the initial translational energy. The energy-corrected sudden approximation was used to determine an "effective" collision length for rotationally inelastic scattering. The scattering is thought to occur predominantly on the repulsive wall of the intermolecular potential, except for the $J=1 \rightarrow J'=0$ transition, which is shown to be sensitive to the depth of the van der Waals attractive well.

I. INTRODUCTION

Rotationally inelastic collisions provide a probe of the anisotropy of intermolecular potentials. Rotational-to-translational ($R \rightarrow T$) energy transfer in atom–diatom collisions is particularly suitable for a comparison of experimental observations and theoretical calculations, since it may often be studied without the complications of competing inelastic processes (vibration-to-translation, or vibration-to-vibration, for example). The dynamics of $R \rightarrow T$ collisions has been the subject to a number of recent studies.[1]

Experimental techniques employed in determining state-to-state $R \rightarrow T$ cross sections have been divided by Toennies[1] into the "energy change" and "state selection" methods. The energy change method utilizes measurements of the change in translational energy brought about by inelastic collisions. This technique was first employed in the study of ion–molecule collisions,[2,3] and has been used by Buck and co-workers,[4] and by Gentry and Giese,[5] in studying $R \rightarrow T$ collisions involving H_2 and its isotopic variants. Recently this approach has been extended to the study of $R \rightarrow T$ in $He + N_2$, CO, and CH_4.[6] In other work, the change of the molecular energy level J is obtained directly by the state selection method, which involves specifying J before the inelastic collision, and measuring it afterwards. This method typically involves the use of electric quadrupole fields to select or detect rotational states in polar molecules, such as CsF and TlF first studied by Toennies and co-workers,[7] and LiH studied by Dagdigian *et al.*[8] Laser induced fluorescence was employed as the detection technique by the latter authors. Lasers have also been used to populate specific vibrational–rotational states in either ground or electronic excited states. The fluorescence of rotational levels adjacent to the laser populated level has been studied in measurements of $R \rightarrow T$ energy transfer in electronically excited Na_2^* by Pritchard and co-workers,[9] in Li_2^* by Vidal,[10] and in the ground electronic state of HF by Lang *et al.*[11] Using an infrared double resonance technique, Hinchen and Hobbs[12] have also studied $R \rightarrow T$ energy transfer in HF. Recently, Bergmann and co-workers[13] have used an optical pumping technique to measure $R \rightarrow T$ differential cross sections for Na_2 in its ground electronic state. Similar measurements have been performed even more recently by Serri *et al.*[14]

In addition to the experimental work indicated above, much theoretical effort has been directed towards an understanding of $R \rightarrow T$ energy transfer. Though this process is conceptually simple for atom–molecule collisions, exact quantum mechanical calculations are still very difficult to perform for most cases. As a result, quantum mechanical approximations,[15] as well as classical trajectory calculations,[16] have been used in computational $R \rightarrow T$ studies. One of the most successful of the quantum mechanical approximations has been the infinite-order sudden (IOS) approximation[17] and modifications.[18,19] Various expressions have been proposed to describe the dependence of $R \rightarrow T$ cross sections on the amount of energy transferred.[16,20–22]

In the present work, an infrared HF chemical laser was employed to select specific rotational levels in either the $v=1$ or $v=2$ vibrational levels of HF molecules in a molecular beam. The fluorescence from levels adjacent to the pumped level, which were populated through inelastic $R \rightarrow T$ collisions with an inert gas scattering partner, were monitored and integral $R \rightarrow T$ cross sections were inferred from the results. The use of molecular beams allowed the collision energy to be varied systematically, thus permitting a direct determination of the effect of collision energy on $R \rightarrow T$ cross sections, and complementing a recent study based on Doppler-shifted laser pumping of $R \rightarrow T$ collisions in $Na_2^* + Xe$.[23] By choosing either the $v=1$ or $v=2$ vibrational state of HF using the present experimental method, the influence of the HF vibrational excitation on $R \rightarrow T$ energy transfer was also investigated. Preliminary qualitative results for the dependence of $R \rightarrow T$ energy

[a] Present address: Argonne National Laboratories, Physics Division, 9700 South Case Avenue, Argonne, Ill. 60439.

 0021-9606/82/020913-18$02.10

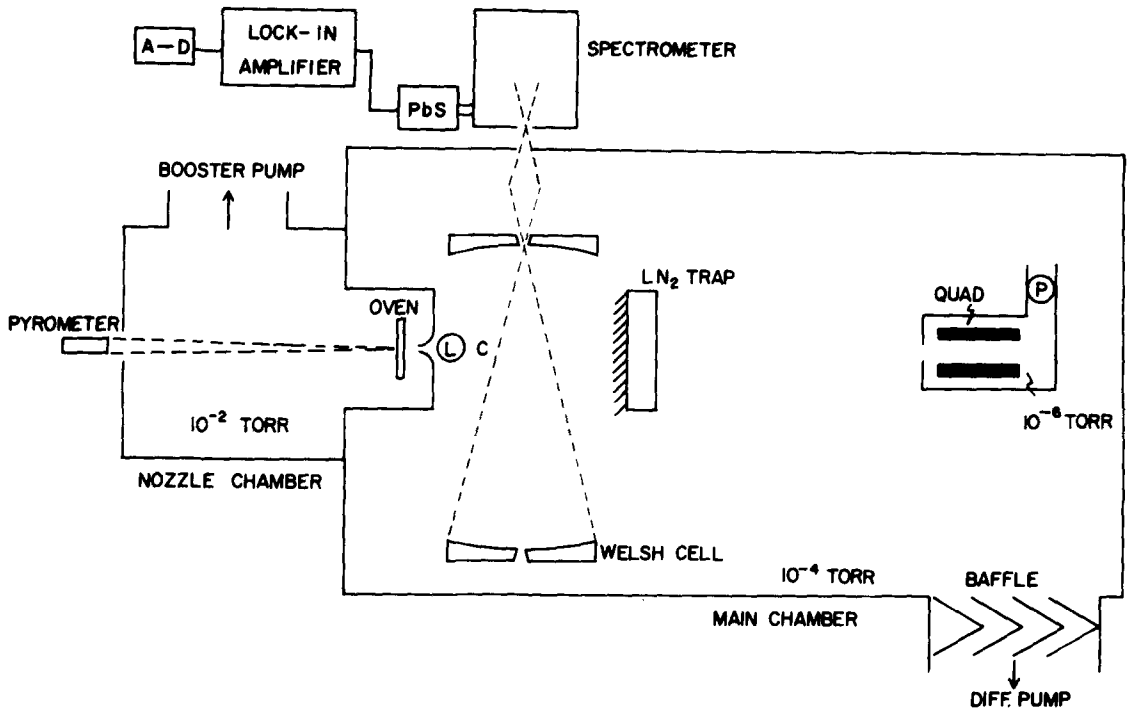

FIG. 1. Schematic diagram of the molecular beam apparatus (not to scale). The laser excitation zone is labeled L; the collision zone C, and the diffusion pump for differential pumping of the quadrupole mass spectrometer chamber P.

transfer on the molecular vibrational level have been reported for $Na_2 + He$ collisions.[13(b)] The present study thus constitutes an investigation of $R \rightarrow T$ cross sections as functions of initial translational, rotational, and vibrational energy for a given system. The work described here is reported in the doctoral thesis of Kutina[24] and was the subject of an earlier Communication from this laboratory.[25]

II. EXPERIMENTAL

The molecular beam apparatus used in our laboratory is shown schematically in Fig. 1. The present version is a modification of the apparatus used in earlier $R \rightarrow T$ studies reported from this laboratory.[26,27] As before, an HF molecular beam was formed in the nozzle chamber by a supersonic expansion from a 0.4 mm diameter nozzle drilled into a graphite oven, whose temperature was measured with an optical pyrometer. After being skimmed, the HF primary beam entered the main (collision) chamber, which contained a multiple-pass Welsh[28] cell for efficient collection of HF infrared emission, and a removable liquid N_2 trap for cryogenic pumping of the HF beam. With the liquid N_2 trap removed, the primary beam traveled into another differentially pumped chamber containing a quadrupole mass spectrometer, for determination of the axial beam velocity.

Figure 2 details the primary and secondary sources, laser excitation of the molecular beam, and collection of

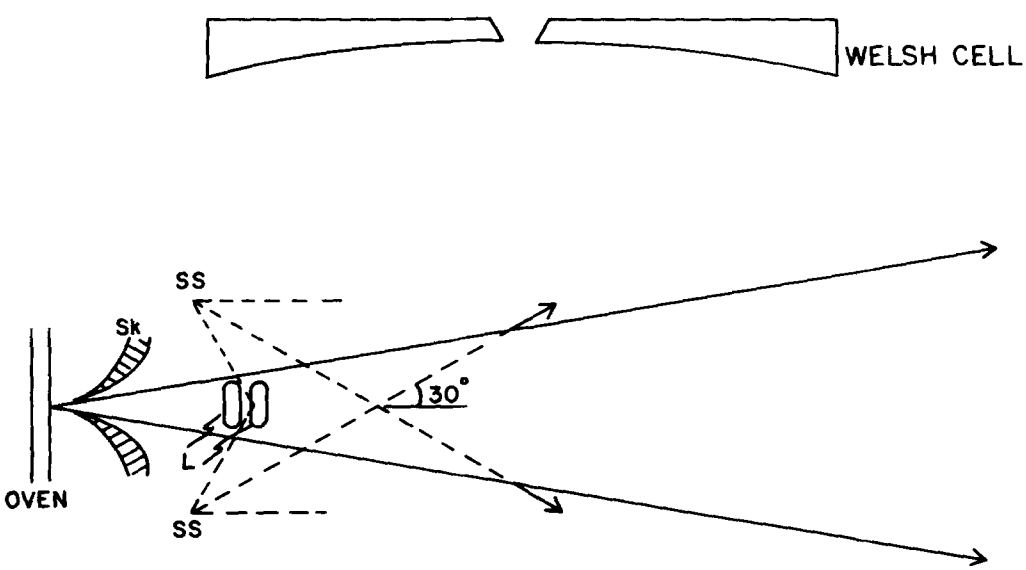

FIG. 2. Schematic diagram of the beam sources, laser excitation zone (L) and the split mirrors at one end of the infrared emission collection Welsh cell (all distances, except for the size of the skimmer, are drawn drawn to scale). The primary beam is shown expanding from the oven through the skimmer Sk. The approximate angular divergencies of the primary beam (solid lines) and secondary source SS (broken lines) are shown. The broken lines terminating in arrows indicate the central lines of the SS.

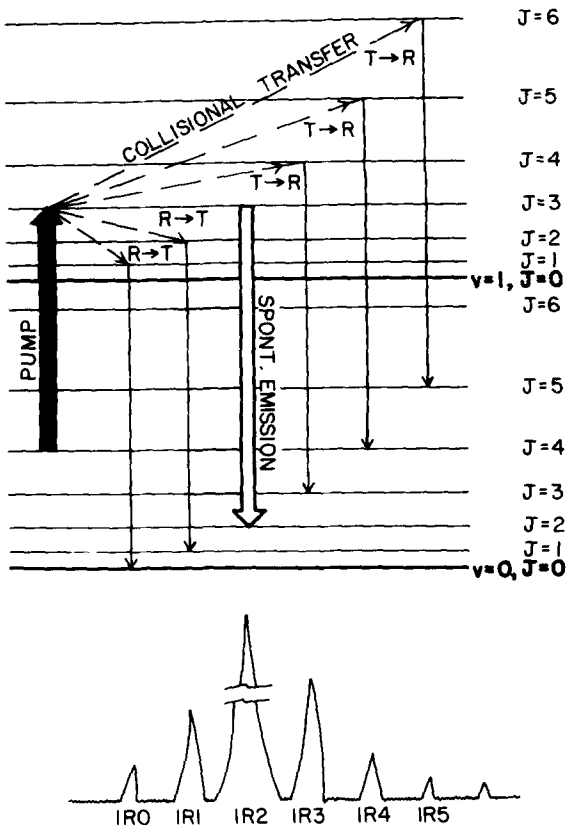

FIG. 3. Schematic representation of the HF energy levels illustrative of the $R \rightleftharpoons T$ energy transfer measurements reported here. In this diagram, the $v=0$, $J=4$ level is pumped to $v=1$, $J=3$ by a cw chemical laser (broad black arrow). Spontaneous emission to $v=0$, $J=2$ (broad arrow) accounts for most of the R-branch emission. Some of the observed collisional $R \rightleftharpoons T$ transfers (broken arrows) populating rotational levels other than $J=3$ in the $v=1$ state, and emitting in the R branch, are denoted as light arrows. The schematic emission spectrum at the bottom of the figure gives the spectroscopic designations of some of the emission lines; the symbol $1R2$ denotes an R-branch line of $v=1 \rightarrow 0$ terminating in $J=2$.

infrared emission. Upon entering the collision chamber, the HF primary beam passed through a multiple-pass absorption cell and was excited to a specific rotational level of the first or second vibrational state by absorption of infrared radiation from a continuous-wave chemical laser. The primary beam then intersected several sprays of secondary gas from a source concentric with the beam axis. Rotationally inelastic encounters experienced by beam molecules were studied by recording changes in the rotational state populations. The population changes were determined from changes in the intensity of vibrational–rotational lines of the HF fundamental emission band, as will be discussed in Sec. III below. The emission was resolved spectrometrically and recorded. Figure 3 illustrates the scheme for pumping a specific vibrational–rotational level of HF, which, upon undergoing rotationally inelastic collisions, gives rise to the (schematic) emission spectrum shown.

The initial collision energy T_i was varied from 4 to 16 kcal/mol by adjusting the fraction of HF in a lighter seeding gas (either He or H_2).[29] The flows of HF and seeding gas were measured by a calibrated Hastings–Raydist mass flowmeter and by Fisher–Porter flow tubes, respectively. The oven pressure was typically 200 Torr for the unseeded beam, and from 400 to 900 Torr for the seeded beams; the oven temperature was maintained at 1800 °K. The peak axial velocities of the HF beams with varying degrees of seeding were determined mass spectrometrically by measuring the phase delay of the mechanically chopped beams.[30] They are given in Table I. This technique did not allow a determination of the Mach number, but a value of $M \approx 10$ may be estimated for our experimental conditions. In Fig. 4, we plot the center-of-mass collision energy distributions in HF + Ar collisions for peak energies near 4, 9, and 16 kcal/mol. Even for the assumed Mach number of $M=6$ used for this calculation,[31] the collision energy distributions are largely nonoverlapping.

It is important to note that the laser pumping of high rotational levels can be accomplished efficiently only if the ground state rotational distribution is not excessively relaxed in the supersonic expansion, since the laser pumps the $v=0$, J state to the $v=1$, $J-1$ state. A typical rotational temperature was 600 °K (oven temperature = 1800 °K) in our work, corresponding to a peak population in $v=0$, $J=3$.

The cw chemical laser[32] used to pump a specific vibrational–rotational level of the HF molecular beam has been described briefly in the excitation of an HF gas cloud.[11] The lasing medium was vibrationally excited HF formed from the reaction $F + H_2 \rightarrow HF + H$. The F atoms were generated by a 1 kW microwave discharge in a flowing $He + SF_6$ mixture. Alumina discharge tubes were found to be much more resistant to attack by hot F atoms than the previously used quartz tubes; tube failure occurred only because of hairline cracks caused by thermal expansion and contraction.

The optical cavity consisted of CaF_2 windows mounted on the laser body at Brewster's angle, producing plane-

TABLE I. Peak center-of-mass collision energies.

%HF/seeding gas	Collision partner, M	v_{HF} (km/s)	v_M (km/s)	V_{rel} (km/s)	T_i (kcal/mol)
100% HF	Ar	1.9	0.35	1.6	4
10% HF/H_2	Ne	3.0	0.50	2.6	8
10% HF/He	Ar	2.6	0.35	2.3	9
25% HF/He	Kr	2.3	0.24	2.1	9
3% HF/H_2	Ar	3.5	0.35	3.2	16

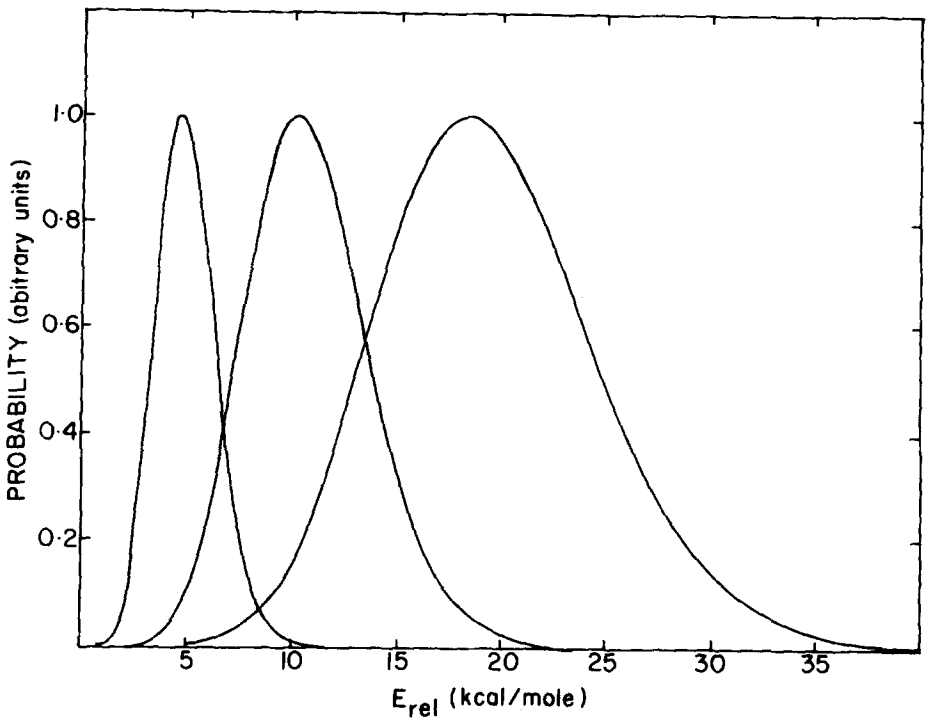

FIG. 4. Calculated center-of-mass collision energy distributions for HF + Ar collisions with three different HF beam velocities. The curves are calculated for a conservative estimate of the Mach number $M=6$; the calculated Mach number of $M\approx 10$ would give somewhat narrower distributions. The peak center-of-mass energies are 4, 9, and 16 kcal/mol, corresponding to no seeding, seeding by 90% He, and seeding by 97% H_2, respectively. The oven temperature was 1800°K.

polarized radiation, a 10% dielectric-coated Ge output coupler, and an intracavity grating mounted in the Littrow configuration for laser line selection. The cavity was kept as short as possible to avoid losses due to intracavity water absorption. The laser was normally operated on the $1P2, 1P3, \ldots, 1P7$ lines ($1P2$ denotes $v=1$, $J=1\rightarrow v=0$, $J=2$), with typical output powers of 0.2–0.8 W. For two-photon excitation of the molecular beam to the $v=2$ state, a mirror was added to the optical cavity and placed so that one particular $v=2\rightarrow 1$ band transition dispersed by the grating (which would normally be lost from the cavity) was reflected back to the grating. The $v=1$ and $v=2$ lasing lines were then coincident both in the lasing medium and in the output beam.[33] The $J=2$ level, pumped by the sequence $v=0$, $J=4\rightarrow v=1$, $J=3\rightarrow v=2$, $J=2$, was the only level in $v=2$ that could be populated in this manner to an extent sufficient for the present $R\rightarrow T$ experiments.

The output laser beam was focused at the entrance slit of a White cell whose axis was perpendicular to both the molecular beam and to the axis of the multiple-pass Welsh cell used for collecting the infrared emission (see Fig. 2). The White cell served as a multiple-pass absorption cell, reflecting the laser beam through the molecular beam approximately 25 times. For the strongest laser lines, this resulted in a measured excitation of ~30% of the $v=0$, J population to $v=1$, $J-1$. This figure of 30% was arrived at in two ways. It could be obtained by comparing the HF ($v=1$) laser excited emission with the corresponding emission from a thermal HF beam coming directly from the hot oven.[34] Alternatively, the fraction in $v=1$ could be calculated from the measured fraction of $v=1$ excited to $v=2$ by a second photon.

The rare gas (Rg) collision partner was introduced into the HF molecular beam path via a series of nozzles of diameter 0.3 mm arranged concentrically around the HF molecular beam axis. The gas flow was kept constant with a Matheson vacuum regulator, and was measured by a Fisher–Porter flow tube. The nozzles were directed in such a way as to converge on the beam axis from all directions, slightly beyond the laser excitation zone and well within the detection viewing region (see Fig. 2). This symmetric arrangement was chosen in order to minimize the net deflection of the primary beam molecules, through elastic encounters. As will be shown, the geometry is not crucial since the Rg atoms have a small velocity relative to the HF. In addition, since the laser excitation zone was also within the detection volume, the HF infrared emission was collected with a roughly invariant efficiency regardless of HF scattering angle. This is an important consideration in the measurement of integral $R\rightarrow T$ cross sections (see Sec. III below).

The Welsh cell mirrors (used for infrared emission collection) were placed so that the molecular beam passed through the region of highest collection efficiency, about 1/3 of the cell length away from the mirrors adjacent to the spectrometer.[35] The infrared emission collected by the Welsh cell was focused onto the entrance slit of a single-pass Perkin–Elmer grating spectrometer, equipped with a PbS detector operated at 77°K. A 0.75 mm spectrometer slit width was chosen as the largest slit capable of fully resolving adjacent R-branch transitions up to $1R9$, corresponding to the highest final state of the measured $R\rightarrow T$ cross sections.

The HF infrared fluorescence was modulated by mechanically chopping the laser beam before it entered the molecular beam apparatus. The modulated signal then represented the vibrationally excited HF produced by the laser, eliminating the constant signal from thermally excited HF and from infrared blackbody radiation, both produced by the hot oven source. This signal was ampli-

fied by a PAR HR-8 lock-in amplifier. The output from the lock-in amplifier was digitized and averaged by a computer to improve the signal-to-noise (S/N) ratio. The best method of measurement was to record the signal continuously, with the spectrometer successively set at selected line peaks.

Vibrational–rotational level populations were obtained by analysis of the R-branch emission spectrum (except for the $J=0$ population, monitored by the $1P1$ or $2P1$ emission). This was preferred to the P branch because of the large P-branch signal due to scattered light from the exciting laser. Populations obtained from R- and P-branch emission intensities differed by $\lesssim 20\%$, for both the $1\rightarrow 0$ and $2\rightarrow 1$ bands. Self-absorption of the emitted HF radiation was found to be negligible under the experimental conditions used (partial pressure of HF $\lesssim 10^{-6}$ Torr). The light path outside the beam apparatus was continually flushed with dry N_2 to eliminate atmospheric water absorption of the $1P1$ and $2R3$ HF emission lines. Since the laser excitation to the $v=2$ state proceeded via $v=1$ excitation, several of the $2\rightarrow 1$ emission lines were overlapped by $1\rightarrow 0$ emission. The latter were selectively removed by a cold gas cell, filled with 50 Torr of HF, which absorbed $> 99.9\%$ of the $1\rightarrow 0$ radiation (but transmitted all $2\rightarrow 1$ emission) over a 2.5 cm absorption path length.

Under the flow conditions employed in this work, the collision chamber pressure was about $1-3\times 10^{-4}$ Torr, mostly due to the Rg collision partner gas load. This was in itself sufficient to induce some $R \rightleftharpoons T$ in the vibrationally–rotationally state-selected HF molecular beam. In order to measure cross sections for $R \rightleftharpoons T$ collisions involving Rg atoms only (as distinct from $R \rightleftharpoons T$ collisions involving background gas, which includes further HF), it was necessary to use a procedure which subtracted the effect of beam-background collisions. This was accomplished by alternating the gas flow between the "active" source (the secondary beam) and a second "dummy" source. The dummy source was located so that its gas flow could not directly intersect the HF beam. Since switching the gas flow between the active and dummy sources did not affect the collision chamber pressure, only those collisions with Rg atoms coming directly from the active source were observed, using a difference method. Alternation of the gas flow was accomplished by a three-way electromagnetic valve under computer control, which also performed the subtraction of $R \rightleftharpoons T$ due to the constant background. Steps were also taken to reduce the pressure of HF in the background gas by cryopumping of the HF beam on a liquid N_2 cold trap (see Fig. 1). "State purity"—i.e., the fraction of HF emitters in the selected vibrational–rotational level—was improved from ~ 70% without liquid N_2 cryopumping to ~ 90% with cryopumping. This was measured with the Rg (argon) flowing from the dummy source into the background.

III. DATA ANALYSIS

If the initial rotational distribution of the HF molecules were localized in only one state J_p, then the cross section for $R \rightleftharpoons T$ energy transfer into another rotational state J', upon collision with a scattering gas atom, would be proportional to $N(J')/N(J_p)$. The symbol $N(J')$ represents the population in level J' transferred from level J_p by $R \rightleftharpoons T$ inelastic collisions, and $N(J_p)$ represents the initial population in level J_p. Measured under the same experimental conditions, the ratio of the population in two rotational levels J' and J'' produced in $R \rightleftharpoons T$ inelastic collisions would be equal to the ratio of cross sections for transfer into these levels from the initially occupied level J_p, i.e.,

$$\frac{N_{J'}}{N_{J''}} = \frac{\sigma_{J_p\text{-}J'}}{\sigma_{J_p\text{-}J''}} . \tag{1}$$

Under actual experimental conditions, this idealized situation is not realized. The initial rotational population is not contained entirely in only one rotational level. Measured fluorescence signals, from which the state populations were inferred, had to be corrected for various experimental factors. The determination of relative cross sections for $R \rightleftharpoons T$ energy transfer from the experimentally measured fluorescence signals is described in the following paragraphs.

The steady-state populations of rotational levels in the $v=1$ or $v=2$ vibrational manifolds were obtained by monitoring the fluorescence signals from the rotational levels in question. As described in Sec. II above, the R-branch transitions were used to determine the population of rotational levels $J=1-10$. The $J=0$ population was determined by observing the $1P1$ or $2P1$ transitions. The fluorescence signal from the pumped level J_p was measured periodically and used to normalize the fluorescence signals from all other levels to the pumped level signal. This procedure corrected for any long term drift in the pump laser or HF flow.

State populations were obtained from corresponding fluorescence intensities using the known Einstein transition probabilities[36] and a factor which corrected simultaneously for the change in sensitivity of the detector with wavelength and the change in efficiency of the detection system optics with wavelength. This correction factor was obtained by scanning the spectrum of a blackbody of known temperature.[26,37]

The transfer of rotational energy into translational energy, or vice versa, results in a change in the velocity with which an HF molecule traverses the viewing region of the detection apparatus. Since the radiative lifetime of vibrationally excited HF is much longer than the transit time of a molecule through the detection system, the observed fluorescence intensity varies inversely with the speed of the emitting molecule. This effect must be considered when comparing the fluorescence intensity from different rotational levels populated by the $R \rightleftharpoons T$ process; it gives rise to a correction term amounting to $\lesssim 20\%$ of the inelastic cross section.

Ideally, this transit time correction should be obtained by convoluting the HF laboratory velocity with the center-of-mass differential cross section (DCS). Since the DCS is not known for the systems presented here we have been guided by computations which show substantial forward scattering for $R \rightleftharpoons T$ using a variety of interaction potentials.[38–40] Examination of the Newton diagram

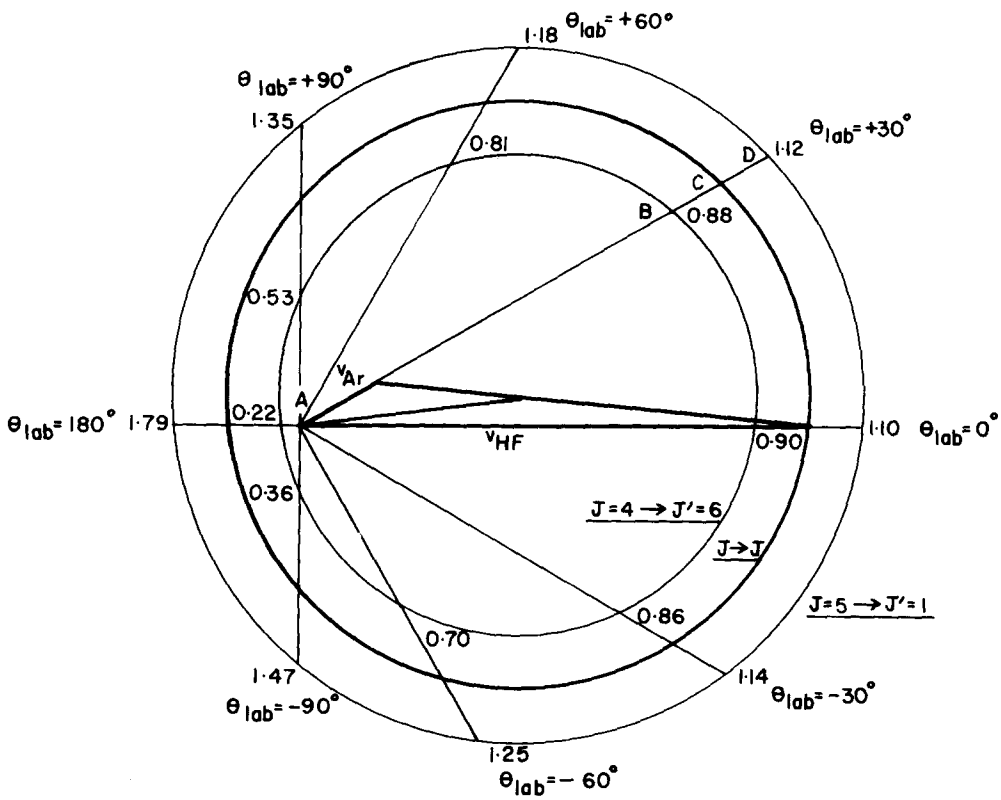

FIG. 5. Velocity vector (Newton) diagram for He+Ar scattering at a collision energy of 4 kcal/mol. The laboratory-frame velocity vectors for HF and Ar, v_{HF} and v_{Ar}, respectively, are shown intersecting at the most probable angle of 30° at the laboratory origin, labeled A. The heavy circle corresponds to elastically scattered HF (labeled $J \rightarrow J$); the inner circle to a $T \rightarrow R$ transition transferring 1.7 kcal/mol (labeled $J=4 \rightarrow J'=6$); and the outer circle to an $R \rightarrow T$ transition, transferring 2.1 kcal/mol (labeled $J=5 \rightarrow J'=1$). The vector labeled AC is the elastically scattered HF laboratory vector for $\theta_{lab}=+30°$. The corresponding vector for $J=4 \rightarrow J'=6$ is labeled AB; that for $J=5 \rightarrow J'=1$, AD. The numbers beside points B and D are the ratios AB/AC and AD/AC, respectively. Similar ratios are given for other laboratory scattering angles θ_{lab} using $J=4 \rightarrow J'=6$ and $J=5 \rightarrow J'=1$ as examples.

in Fig. 5 shows that the correction factor, which depends on the ratio of v_{lab} for inelastically scattered HF to v_{lab} for elastically scattered HF, does not vary significantly in the range $|\theta_{lab}| < 60°$. The corrections are largest for the $T_i = 4$ kcal/mol case where, as noted, they amount to $\lesssim 20\%$. The velocity (transit time) corrections are listed for all relevant $J \rightarrow J'$ transitions in Table II.

The Welsh cell used to collect the fluorescence radiation does not collect radiation originating from different regions within its boundaries with equal efficiency.[35] If, for example, one assumes scattering of HF(J'), following inelastic collision, through 45° in the laboratory frame, the intensity coming from the Welsh cell is reduced by approximately 35%. (Scattering at 45° is the worst case; the effect is as small as this owing to the fact that molecules leave the scattering center along the Welsh cell axis as well as perpendicularly to it; those that move along the cell axis have more time in which to emit.) Given the modest size of this effect even for large θ_{lab}, we can ignore the distortion that *variation* in this effect produces in the relative values of $\Delta N(J')$, which govern the relative inelastic cross sections.

Under actual experimental conditions, the entire population of the $v=1$ vibrational level was not contained solely in the pumped level J_p. Due to collisions with background HF, as well as the scattering gas and seeding gas in the background, some redistribution of the pumped level population occurred before the scattering region was reached. The "purity" of the pumped level, as noted in Sec. II, was typically 90%; hence the correction for "impurity" described below was not severe.

When the inert gas flow was switched from the dummy secondary source to the active secondary source, concentric with the HF primary beam (see Sec. II), a change in the rotational levels neighboring the pumped level was observed. This change in population, $\Delta N(J')^{obs}$, was determined from the corresponding change in the fluorescence intensity shown in Fig. 6. The observed population change $\Delta N(J')^{obs}$ in a level J' was the result of two competing contributions: collisional transfer from levels J (including J_p) into J' and transfer out of J' into other

TABLE II. Emitter residence time correction factors for HF+Ar at $T_i = 4$ kcal/mol.[a]

Final state	Initial state J					
J'	1	2	3	4	5	6
0	1.01	1.02	1.05	1.08	1.11	···
1	1.00	1.01	1.04	1.07	1.10	···
2	0.98	1.00	1.02	1.05	1.09	1.13
3	0.96	0.98	1.00	1.03	1.07	1.11
4	0.92	0.94	0.97	1.00	1.04	1.08
5	0.87	0.89	0.92	0.96	1.00	1.05
6	0.81	0.83	0.86	0.90	0.95	1.00
7	b	b	0.78	0.83	0.89	0.94
8	b	b	b	b	0.80	0.86

[a]The collected emission intensity is inversely proportional to the emitter velocity; these corrections are obtained with the assumption of forward scattering in the laboratory frame.
[b]These cross sections correspond to a transfer of > 50% of the initial translation energy and are not included in the data analyses.

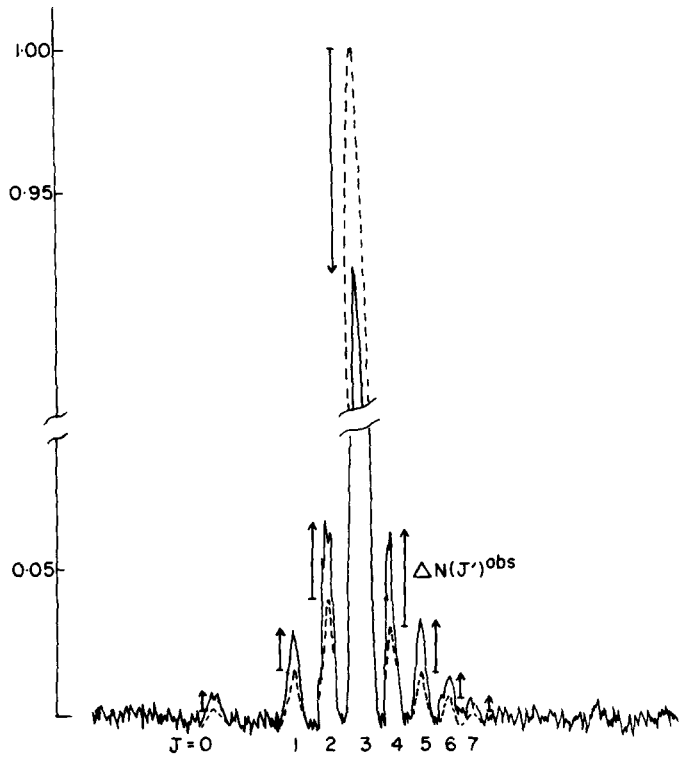

FIG. 6. Example of an HF fluorescence spectrum with the laser tuned to pump the $v=1$, $J=3$ level (1P4 laser transition). Note the scale change for emission from $J=3$. Dotted lines show the appearance of the spectrum with Ar flowing through the "dummy" source, with the solid lines corresponding to Ar flowing through the "active" source. The downward arrow for the pumped level $J=3$ shows the $R \rightarrow T$ transfer from $J=3$ to all other levels J'. The corresponding increases in the J levels are shown by upward arrows, labeled $\Delta N(J')^{obs}$. These spectra are single traces of the HF 1P1 ($J=0$) and R branch ($J \leftrightarrow 0$) emission lines, before being computer averaged for improvement of the signal-to-noise ratio.

rotational states. Assuming single collision conditions and a negligible change in the $v=1$ population due to $T \rightarrow V$ energy transfer (both assumptions to be justified later), we have

$$\Delta N(J')^{obs} = \sum_{J \neq J'} N(J) P_{J \rightarrow J'} - \sum_{J \neq J'} N(J') P_{J' \rightarrow J} , \qquad (2)$$

where $P_{J \rightarrow J'}$ is the probability of the $R \rightarrow T$ process $HF(J) \rightarrow HF(J')$. The right-hand side of this equation is dominated by the term, within the first summation, representing transfer from the pumped level, i.e., $N(J_p)P_{J_p \rightarrow J'}$. If we denote the transfer from the pumped level to level J' by $\Delta N(J')$, then we may write

$$\begin{aligned} \Delta N(J') &= N(J_p) P_{J_p \rightarrow J'} \\ &= \Delta N(J')^{obs} - \Bigg(\sum_{J \neq J', J_p} N(J) P_{J \rightarrow J'} \\ &\quad - N(J') \sum_{J \neq J'} P_{J' \rightarrow J} \Bigg) . \end{aligned} \qquad (3)$$

The bracketed term on the right-hand side of this equation constitutes a correction term for the impurity of the initial state. The correction term was usually small compared to $\Delta N(J')^{obs}$. The transfer probabilities $P_{J \rightarrow J'}$ required to evaluate the correction term were estimated to a first approximation as $\Delta N(J')^{obs}/N(J_p)$; the $N(J)$ populations also required to evaluate the correction term were measured during the experiment simultaneously with the $\Delta N(J')^{obs}$. Microscopic reversibility was used to obtain unobserved transfer probabilities (e.g., out of $J=0$) from observed ones. The correction term was then calculated and applied in calculating a second approximation to the transfer probabilities. This iterative procedure rapidly converged to a self-consistent solution for the transfer probabilities. The corrections amounted to less than 20% of the observed population change for all transitions except for the $J=1 \rightarrow J=0$ transition, for which the correction was as large as 30% in the case of HF + Ar at $T_i = 16$ kcal/mol.

To investigate any possible contribution to population changes due to $T \rightarrow V$ energy transfer, an attempt was made to observe emission due to $v=2$ populated by high energy collisions between HF ($v=1, J=3$) and Kr. The peak center-of-mass collision energy was 18 kcal/mol with the half-width of the distribution extending to 24 kcal/mol. Although a significant fraction of the collisions were above the threshold for vibrational excitation ($\Delta E = E_{v=1,J=3} - E_{v=2,J=3} = -10.8$ kcal/mol) by approximately a factor of 2, any population in $v=2$ produced by $T \rightarrow V$ was below the sensitivity of the detection system. With a S/N ratio of ~100 for $R \rightarrow T$ processes under the same experimental conditions, we estimate a $T \rightarrow V$ cross section of less than 1% of the cross section for the rotational transfer $(v=1, J=3) \rightarrow (v=1, J=2)$. The same qualitative statement most likely applied to the $v=1 \rightarrow v=0$ transition, since the cross sections for $T \rightarrow V$ and $V \rightarrow T$ would not differ dramatically at collision energies so far above threshold.[41]

For the quantity $\Delta N(J')^{obs}$ to be the result of single rotationally inelastic collisions with the scattering gas, multiple $R \rightarrow T$ collisions must constitute an insignificant fraction of all such collisions. This was assured by using a Rg flow low enough to deplete the pumped level by < 10%. Since this represented the total transfer from J_p to all J', the effect of multiple $R \rightarrow T$ collisions is also < 10%.

In view of the absence of multiple rotationally inelastic collisions, the transfer probabilities $\Delta N(J')/N(J_p)$ should have a linear dependence on the density of the scattering gas. In other studies,[11,42] we have observed that the scattering gas density was proportional to its in-flow. Figure 7 demonstrates the linearity of the transfer probabilities with scattering gas flow for the system $HF(J_p = 1)$ + Ar at a center-of-mass collision energy of 4 kcal/mol. The plots are all linear up to 40 μmol/s. Similar plots were also obtained for the remainder of the systems studies.

In earlier $R \rightarrow T$ work,[26,27] it was shown that elastic collisions could cause the infrared emitters to be slowed down in the laboratory frame, thus increasing the apparent population in all J' levels, including the pumped level J_p. Whatever elastic scattering occurred in this work did not affect the efficiency with which the infrared emitters were detected. This may be seen by comparing the population of emitters lost from the pumped level J_p,

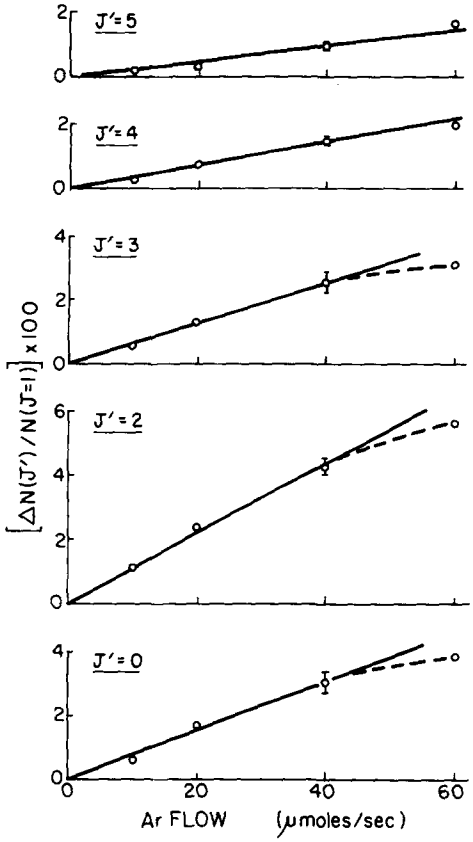

FIG. 7. Plots of population changes $\Delta N(J')$ vs Ar in flow for HF+Ar at $T_i = 4$ kcal/mol for various final rotational states J' Typical error bars, corresponding to one standard deviation, are shown for the data at 40 μmol/s.

to the sum of populations appearing in adjacent levels J'. Emitters from level J_p would all be slowed down by the elastic effect and the resultant increase in intensity would partially offset the depletion of this level by the scattering gas. Experimentally, however, we observed the depletion of level J_p to be only slightly less than the sum of the populations transferred into the adjacent levels J'.

IV. RESULTS AND DISCUSSION

A. Results

Once the fluorescence data were corrected, as discussed in Sec. III above, $\Delta N_{J'}/\Delta N_{J''}$ gave relative cross sections for transfer to levels J' and J''. Although some of the corrections applied are somewhat crude, they are of sufficiently small magnitude that the relative cross sections are estimated to be accurate to within ~20%.

It was found, in general, that the relative cross sections for $R \rightarrow T$ energy transfer were not significantly affected by changing either the collision energy or the collision partner; see Tables III and IV. The exceptions were the $J=1 \rightarrow J'=0$ transition, and large upward transfers of energy with an initial collision energy of 4 kcal/mol. In the latter case, a significant fraction of the collisions took place with energies at or below the threshold energy for the upward transitions (see Fig. 4). It seems probable that the increased $\sigma_{J \rightarrow J'}$ with collision energy in going from 4 to 9 kcal/mol was simply due to the fact that at 9 kcal/mol all the collisions had the requisite energy to give large positive ΔJ.

The cross section for $J=1 \rightarrow J'=0$ was thus the only observed cross section which was significantly affected by changing the collision partner or collision energy. The cross section decreased by a factor of 1.7 in going from Ar and Kr as collision partners to Ne, at a constant collision energy of 9 kcal/mol. It also decreased by a factor of 2.7 in increasing the collision energy from 4 to 16 kcal/mol, with Ar as the collision partner.

Since it was not known to what extent the scattering gas density was altered in changing the collision partner, the cross section matrices were arbitrarily normalized to the $J=1 \rightarrow J'=2$ cross section. Each cross section is the result of an average of 4–8 individual "data points," which are themselves the average of 3–5 consecutive difference measurements, $\Delta N(J')^{obs}$, made under computer control. The longer data accumulation times were used in measuring the larger rotational jumps, to compensate for their lower S/N ratios. One standard deviation of the data points comprising each cross section is generally $\pm 10\%$ for small ΔJ transitions, increasing to $\pm 30\%$ for the largest ΔJ transitions observed.

The $R \rightarrow T$ cross sections exhibit the general trend of a rapid decrease with increasing ΔJ for small ΔJ and a more gradual decrease for larger ΔJ. This trend is illustrated graphically in Fig. 8 for the system HF + Ar at $T_i = 9$ kcal/mol.

B. Empirical models

To account for the observed relaxation pattern in hydrogen halides, Polanyi and Woodall[20] proposed an expression in which the cross section for $R \rightarrow T$ energy transfer was an inverse exponential function of the "energy gap," i.e., the magnitude of the energy transferred. When made to obey microscopic reversibility, this expression is written as[16(b)]

$$\sigma_{J \rightarrow J'} \propto N(T_f/T_i)^{1/2} \exp(-C|\Delta E_{JJ'}|) , \quad (4)$$

where $\Delta E_{JJ'} = E_J - E_{J'}$ and C is an experimentally determined constant. The factor N is an angular momentum statistical factor; $N = N_\Delta = 2J' + 1$ is appropriate for m_J randomization and $N = N_0 = (2J_< + 1)/(2J + 1)$, where $J_<$ is the lesser of J and J', is appropriate for m_J conservation.

With $N = N_\Delta$, the single parameter C of the "exponential-gap" model adequately described the entire rotational relaxation pattern from any given initial rotational distribution.[20] The expression had the characteristic that $\sigma_{J \rightarrow J'}$ depended only on $|\Delta E_{JJ'}|$ and not on the initial J. The parameter C governed the energy dependence of the probability of $R \rightarrow T$ energy transfer; a lower value of C indicated that the transfer probability diminished less steeply with increasing $|\Delta E_{JJ'}|$. A similar exponential expression for $R \rightarrow T$ energy transfer, also with $N = N_\Delta$, was obtained subsequently through a suprisal analysis of inelastic collisions.[43] The two expressions were shown to be equivalent,[44] thus providing a theoretical basis for the purely empirical, one-parameter exponential ex-

TABLE III. Cross section matrix for HF+Ar at T_i=4, 9, and 16 kcal/mol.[a]

Final State J'	T_i kcal/mol	Initial state J 1	2	3	4	5	6
	4	1.09	0.28	0.108	0.082	0.064	···
0	9	0.77	0.30	0.105	···	0.042	···
	16	0.40	0.26	0.092	···	····	···
	4		0.73	0.33	0.18	0.12	···
1	9		0.74	0.33	0.16	0.11	···
	16		0.64	0.35	···	···	···
	4	1.00		0.78	0.43	0.21	0.14
2	9	1.00[a]		0.73	0.34	0.22	···
	16	0.97		0.68	···	···	···
	4	0.56	0.80		0.78	0.38	0.25
3	9	0.49	0.76		0.66	0.31	···
	16	0.56	0.71		0.77	···	···
	4	0.26	0.42	0.82		0.74	0.39
4	9	0.24	0.41	0.66		0.71	···
	16	0.23	0.36	0.62		0.64	
	4	0.15	0.20	0.35	0.69		0.63
5	9	0.14	0.21	0.31	0.54		···
	16	0.14	0.19	0.31	0.50		···
	4	0.092	0.10	0.14	0.26	0.60	
6	9	0.118	0.12	0.17	0.25	0.52	
	16	···	0.12	0.17	···	0.49	
	4	0.057[b]	0.044[b]	0.058	0.098	0.23	0.50
7	9	0.089	0.062	0.101	0.170	0.23	···
	16	···	0.088	0.095	···	···	···
	4	0.015[b]	0.016[b]	0.017[b]	0.039[b]	0.050	0.11
8	9	0.064	0.059	0.054	0.078	0.121	···
	16	···	···	···	···	···	···
	4	···	···	···	···	···	0.039[b]
9	9	0.044	0.039	0.043	···	0.069	···
	16	···	···	···	···	···	···

[a]The cross sections are arbitrarily normalized to $\sigma(J=1\rightarrow J'=2)\equiv 1.000$ at $T_i=9$ kcal/mol.
[b]See note b of Table II.

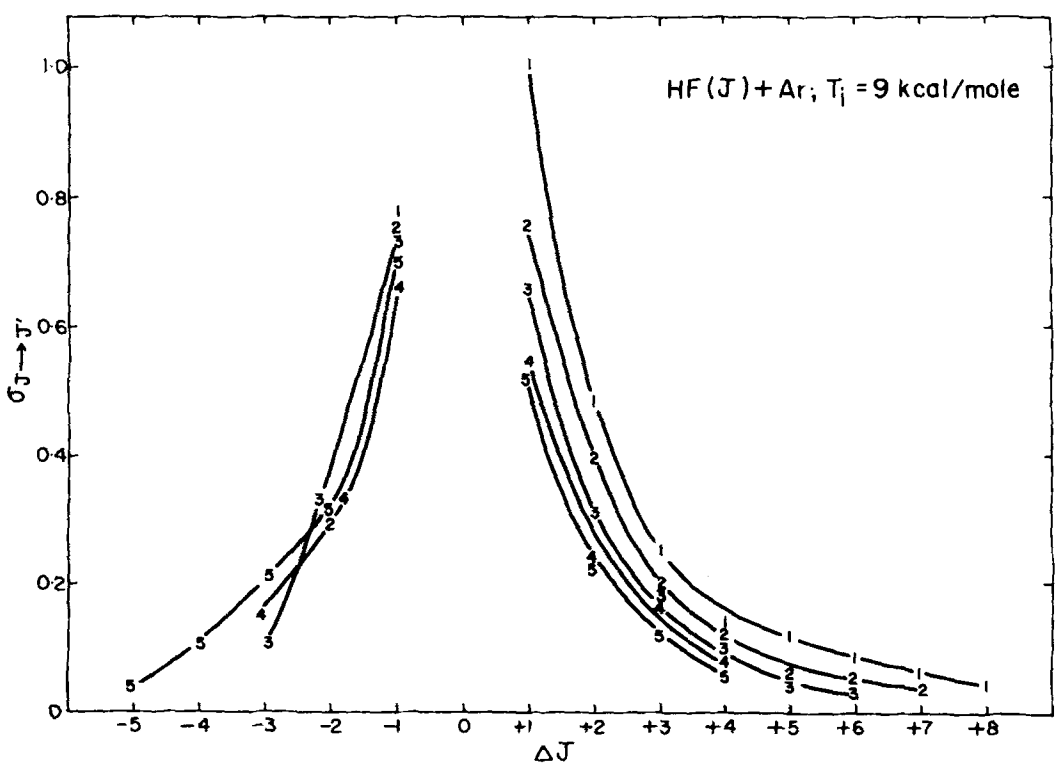

FIG. 8. Cross sections $\sigma_{J\rightarrow J'}$ for HF+Ar at T_i = 9 kcal/mol plotted vs the change in rotational state $\Delta J=J'-J$. Points on the various curves, labeled by the initial HF rotational state J, are joined for clarity of data presentation.

TABLE IV. Cross section matrix for HF+Ne, Ar, Kr at T_i = 9 kcal/mol.[a]

Final state J'	Collision Partner M	Initial state J 1	2	3
	Ne	0.44	0.26	0.14
0	Ar	0.77	0.30	0.11
	Kr	0.76	0.27	0.12
	Ne		0.70	0.41
1	Ar		0.74	0.33
	Kr		0.71	0.33
	Ne	1.00[a]		0.79
2	Ar	1.00[a]		0.73
	Kr	1.00[a]		0.67
	Ne	0.69	0.84	
3	Ar	0.49	0.76	
	Kr	0.51	0.74	
	Ne	0.26	0.49	0.76
4	Ar	0.24	0.41	0.66
	Kr	0.24	0.32	0.57
	Ne	0.17	0.22	0.41
5	Ar	0.14	0.21	0.31
	Kr	0.17	0.19	0.28
	Ne	0.19	0.12	0.20
6	Ar	0.12	0.12	0.17
	Kr	0.10	0.12	0.18
	Ne	0.115	0.093	0.12
7	Ar	0.089	0.062	0.10
	Kr	0.075	0.084	0.11
	Ne	0.087	0.063	0.085
8	Ar	0.064	0.059	0.054
	Kr	0.080	0.056	0.060
	Ne	0.047	0.037	0.056
9	Ar	0.044	0.039	0.043
	Kr	...	0.041	0.035

[a]The cross sections are arbitrarily normalized to $\sigma(J=1\rightarrow J'=2) \equiv 1.000$ for each collision partner; T_i=8 kcal/mol for HF+Ne.

pression. In succeeding years, the results of a number of theoretical studies in $R \rightleftharpoons T$ energy transfer—quantal close-coupling calculations and classical trajectories—were found to be approximately consistent with the exponential gap relation.[21] More recently, theoretical[16(a)] and experimental[9,22,25] studies have drawn attention to a limitation of the exponential-gap expression, namely its tendency to underestimate the probability of large ΔJ transitions. Pritchard and co-workers[9,22] introduced an alternative relationship that embodied a less rapid fall-off in $\sigma_{J\rightarrow J'}$ with $\Delta E_{JJ'}$ (and hence with increasing ΔJ),

$$\sigma_{J\rightarrow J'} \propto N(T_f/T_i)^{1/2} |\Delta E_{JJ'}|^{-\gamma}, \tag{5}$$

where the single parameter γ was used successfully to describe state-to-state $R \rightleftharpoons T$ cross sections. In this study of $Na_2^* + Xe$, the use of the $N = N_0$ statistical factor was found to remove an asymmetry between upward ($J < J'$) and downward ($J > J'$) cross sections which was observed with the N_Δ factor.

As a test of the exponential-gap expression [Eq. (4)], the state-to-state cross sections for HF + Ar at $T_i = 9$ kcal/mol are plotted on a semilog plot in Fig. 9. The nonlinearity of this plot is indicative of the failure of the exponential gap expression to scale properly the $R \rightleftharpoons T$ cross sections over the full range of $|\Delta E_{JJ'}|$. A test of the "power gap" expression [Eq. (5)] is shown in Fig. 10, also for the case of HF + Ar at $T_i = 9$ kcal/mol. The linearity of this plot is in striking contrast to the curvature of the previous plot (Fig. 9), both of which utilized the $N = N_\Delta$ angular momentum statistical factor, and establishes the power gap expression as a more satisfactory scaling relationship for $R \rightleftharpoons T$ energy transfer in hydrogen halides.

The value of the exponent γ of Eq. (5) is shown in Fig. 10 to be independent of the initial rotational level, but dependent on the sign of $\Delta E_{JJ'}$. Both values of γ are consistent with values for other systems previously ana-

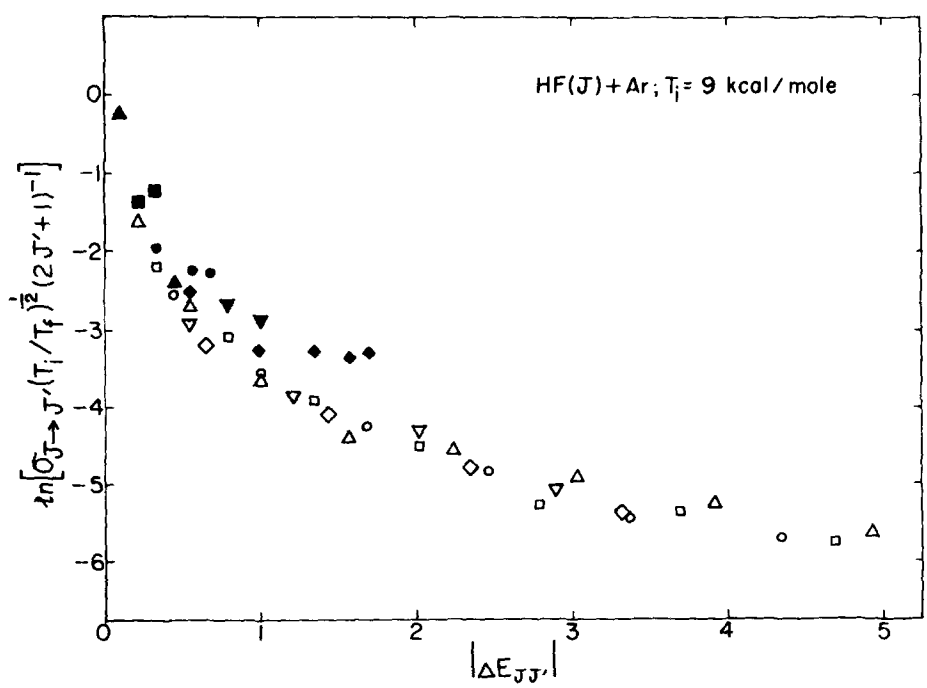

FIG. 9. Semilog plot of $R \leftrightarrow T$ data for HF+Ar with T_i = 9 kcal/mol, assuming angular momentum statistics appropriate for m_J randomization (N_Δ). A linear plot would confirm exponential-gap behavior; see Eq. (4). Filled symbols–downward transitions ($J > J'$); open symbols-upward transitions ($J < J'$); triangles–J=1; squares—J=2; circles—J=3; inverted tirangles—J=4; diamonds—J=5.

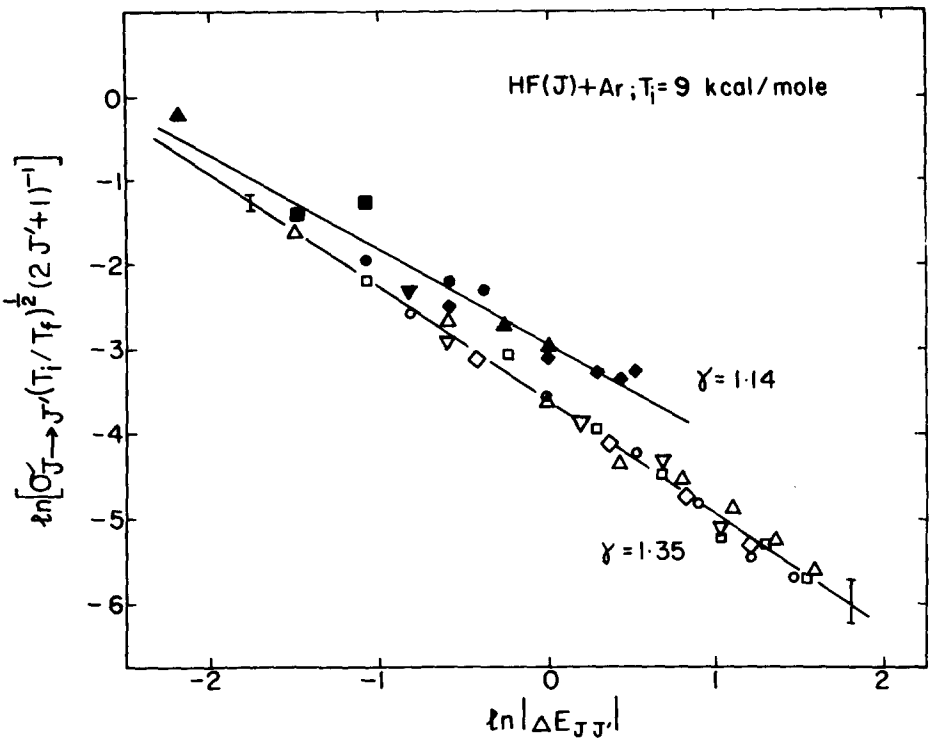

FIG. 10. Log–log plot of $R \leftrightarrow T$ data for HF = Ar with $T_i = 9$ kcal/mol, assuming angular momentum statistics appropriate for m_J randomization (N_Δ). The linear plot confirm power gap behavior; see Eq. (5). The best-fit lines were obtained by treating upward and downward transitions as separate sets of data, resulting in the separately labeled values of the parameter γ of Eq. (5). Error bars are for one standard deviation, generally ± 10% for the larger cross sections, and ± 30% for the smaller ones. Other symbols as in Fig. 9.

lyzed in this manner, which ranged from 0.7 to 1.6 and were independent of the initial rotational level.[9,22]

Pritchard and co-workers had found for $Na_2^* + Xe$ that a different γ was obtained for upward and downward $R \rightarrow T$ transitions, until they introduced the assumption of $\Delta m_J = 0$.[9] When we employ this selection rule, we obtain the results shown in Fig. 11. Clearly, the asymmetry between upward and downward transitions observed in our study is not removed by the single assumption that $\Delta m_J = 0$. There are, however, important differences between our experimental conditions and those of Pritchard's group, stemming from the fact that they work in bulb conditions, whereas we work with a (supersonic) beam of HF. They can assume an initial equilibrium distribution over m_J states—i.e., an equal population in all such states. We cannot assume this. The possible consequences of nonequilibrium distributions over m_J states are examined in Sec. IV C below, along with the consequences of $\Delta m_J \neq 0$ for HF + Rg $R \rightarrow T$ collisions.

Figure 12 shows that the relative $R \rightarrow T$ cross sections measured in this work are independent of collision en-

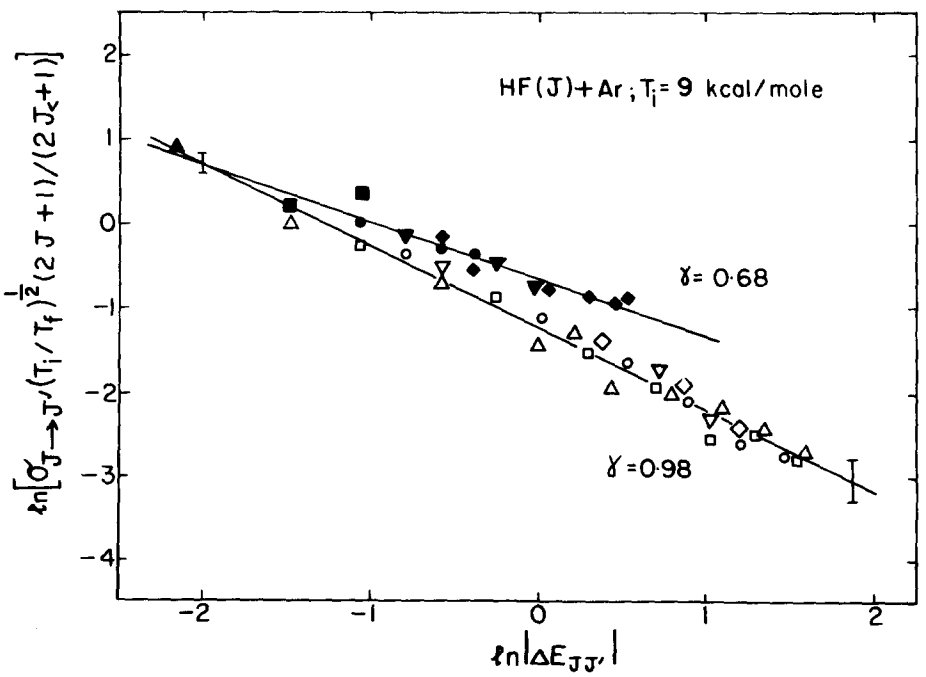

FIG. 11. Same plot as in Fig. 10, but assuming angular momentum statistics appropriate for m_J conservation (N_0).

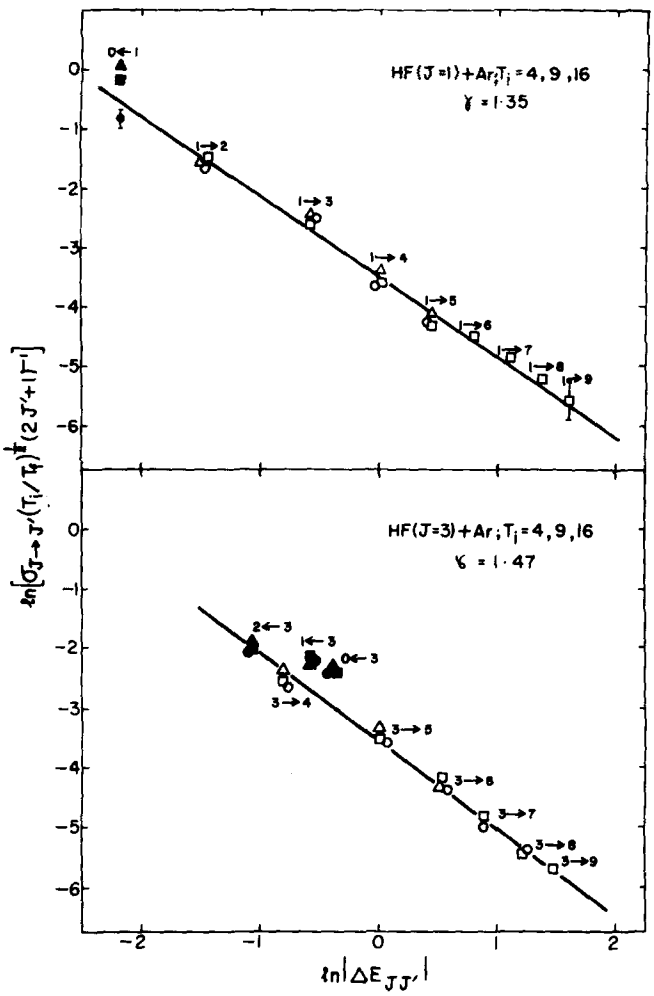

FIG. 12. Varying collision energy: log–log plot of HF + Ar $R \leftrightarrow T$ cross sections for two initial rotational states J. Upper panel: $J=1$; lower panel: $J=3$. Filled symbols—downward transitions ($J>J'$); open symbols—upward transitions ($J<J'$); triangles—$T_i=4$; squares—$T_i=9$; circles—$T_i=16$ kcal/mol. The lines represent linear least-squares fits to Eq. (5), using only the downward cross sections. Error bars are typical for one standard deviation of the measured cross sections.

ergy from $T_i=4$–16 kcal/mol for HF($J=1$) + Ar and for HF($J=3$) + Ar. A similar insensitivity to change in collision energy was noted for N_2 + Ar in an analysis of computed cross sections.[21(b)] A recent experimental study of the effect of collision energy on $R \leftrightarrow T$ energy transfer in Na_2^* + Xe over a somewhat lower range of collision energies, governed by the Doppler breadth of laser excitation of the $Na_2^*(J)$, showed only modest changes in $\sigma_{J\to J'}$ with T_i.[23]

The exception, in our work, is $\sigma_{1\to 0}$ which decreased by a factor of 2.7 with an increase in collision energy from $T_i=4$ to 16 kcal/mol (Fig. 12 and Table III).

The relative cross sections we measured, in general, are insensitive also to the nature of the collision partner, Ne, Ar, or Kr; see Fig. 13 and Table IV. The exception, once again, is $\sigma_{1\to 0}$. At $T_i=9$ kcal/mol, $\sigma_{1\to 0}$ decreases by a factor of 1.7 in going from Kr or Ar to Ne.

It should be stressed that we are speaking of the invariance of *relative* cross sections with T_i and with the Rg collision partner. In terms of Eq. (5), we can express this as an invariance of γ. Invariance of γ with collision partner has also been observed in a recent study of $R \leftrightarrow T$ cross sections for Na_2^* + He, Xe collisions.[9]

In previous work on $R \leftrightarrow T$ transfer performed in this laboratory, without laser selection of initial J states, analysis of the results was only possible through application of a model for $\sigma = fn(J, J')$.[26,27] The model used was the exponential gap expression [Eq. (4)]. As we have shown here for the same system, the exponential gap expression performs poorly for large ΔJ. In our earlier work, we selected the adjustable parameter C in Eq. (4) to give the best fit over the full range of J values observed. At enhanced collision energy this range of J increased, necessitating a change in C. This is illustrated in Fig. 14 for individual $\sigma_{J\to J'}$, obtained in the present (initial state-selected) experiments. Because of the curvature of the semilog plot corresponding to the exponential gap expression, a lower value of C is re-

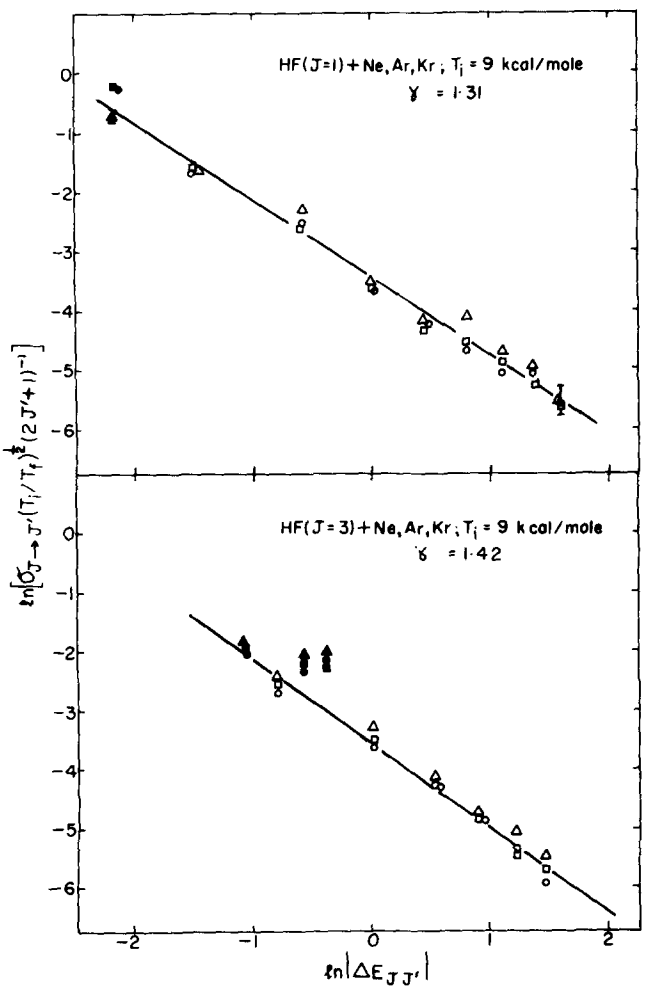

FIG. 13. Varying collision partner: log–log plot of HF + Rg $R \leftrightarrow T$ cross sections for two initial rotational states J, with $T_i=9$ kcal/mol. Upper panel: $J=1$; lower panel: $J=3$. Triangles—Rg = Ne (T_i is actually 8 kcal/mol for HF + Ne); squares—Rg = Ar; circles—Rg = Kr. Other symbols as in Fig. 12.

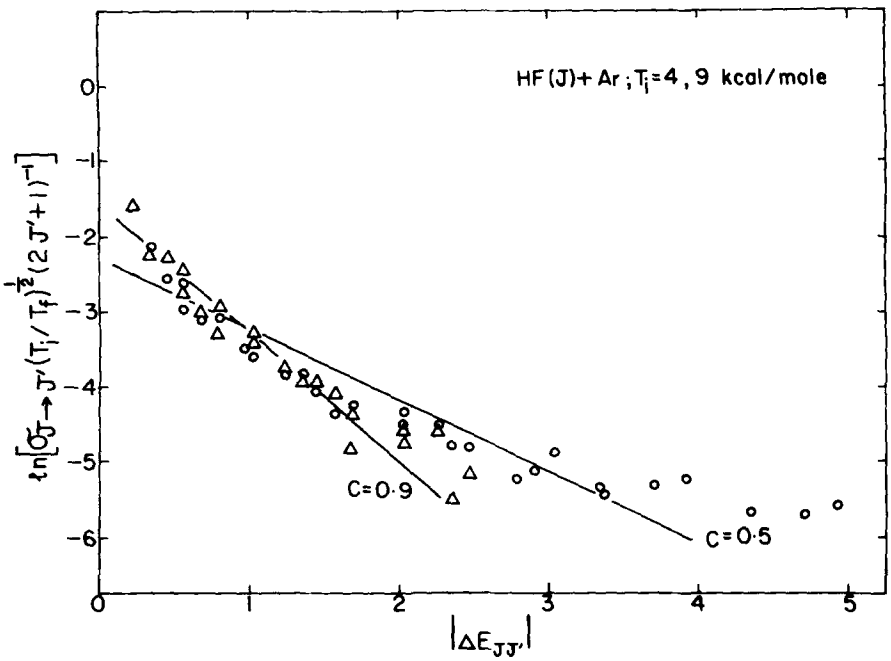

FIG. 14. Semilog plot of state-to-state cross sections for HF + Ar at two collision energies: triangles—$T_i = 4$; circles—$T_i = 9$ kcal/mol. The lines were obtained by fitting the data to the exponential-gap expression [Eq. (4)], and result in the labeled values of the parameter C. The decreasing value of C at higher collision energy T_i results from the presence of larger ΔJ transitions rather than from any overall change in the cross sections (see text).

quired to fit results extending out to large ΔJ. Clearly the decrease in C with increased collision energy is a consequence of the attempt to make the exponential gap expression give acceptable values for the cross sections of large ΔJ's, which evidence themselves at high center-of-mass collision energy. When these same nonstate-selected $R \rightleftharpoons T$ data are fitted to the power gap expression of Eq. (5), we find that the best-fit parameter γ is independent of collision energy. This result is in agreement with the state-selected results reported here.

C. Corresponding upward and downward transitions

It was noted in Sec. IV B above, that the upward ($J < J'$) and downward ($J > J'$) transitions, though they both scale according to Eq. (5), fell onto two distinct lines having different slopes γ (see Fig. 10).

According to the principle of microscopic reversibility, the degeneracy-averaged cross sections for upward and downward transitions between rotational states i and f are related by the expression

$$\sigma_{i\to f} = (T_f/T_i)(g_f/g_i)\sigma_{f\to i} , \qquad (6)$$

where g_i and g_f are the angular momentum degeneracies of the rotational states i and f, and T_i and T_f are the initial and final translational energies, respectively, in the transition $i \to f$. Inspection of Eq. (5) shows that it will only satisfy this microscopic reversibility relation if $|\Delta E_{J,J'}|^{-\gamma}$ in Eq. (5) cancels for the corresponding upward and downward transition; this cancellation requires a single value of γ.

The apparent failure of these results to satisfy degeneracy-averaged microscopic reversibility has been assessed by calculating downward cross sections by microscopic reversibility from the corresponding measured upward cross sections [Eq. (6)]. The calculated values are found to be less than the measured downward cross sections by (in the worst case) as much as 61% of the measured downward cross section. The percentage discrepancies of the calculated cross sections from the measured downward cross sections are shown in Table V for HF + Ar at two center-of-mass collision energies. Inspection of this table shows that these discrepancies are largest for large ΔJ, suggesting that either the translational energy of rotational degeneracy factors of Eq. (6) may not be correct. We proceed by discussing possible errors in these factors.

The calculated downward cross sections are for the reverse of the transition $i, T_i \to f, T_f$; i.e., they correspond to $f, T_f \to i, T_i$. The initial and final translational energies of this calculated downward cross section are not equivalent to those of the corresponding measured downward cross section. As an example, consider the downward transition $J = 5 \to J' = 1$ at an initial collision

TABLE V. Percentage deviations of calculated[a] from measured downward cross sections for HF + Ar at $T_i = 4$ and 9 kcal/mol.

Final state J'	T_i kcal/mol	Initial state J 2	3	4	5	6
1	4	−13	−18	−34	−42	···
	9	−17	−33	−46	−61	···
2	4		−20	−31	−28	−40
	9		−23	−27	−49	···
3	4			−9	−19	−48
	9			−18	−29	···
4	4				−12	−33
	9				−33	···
5	4					−5
	9					···

[a]From microscopic reversibility, assuming m_J randomization during $R \leftrightarrow T$ collisions; Eq. (6).

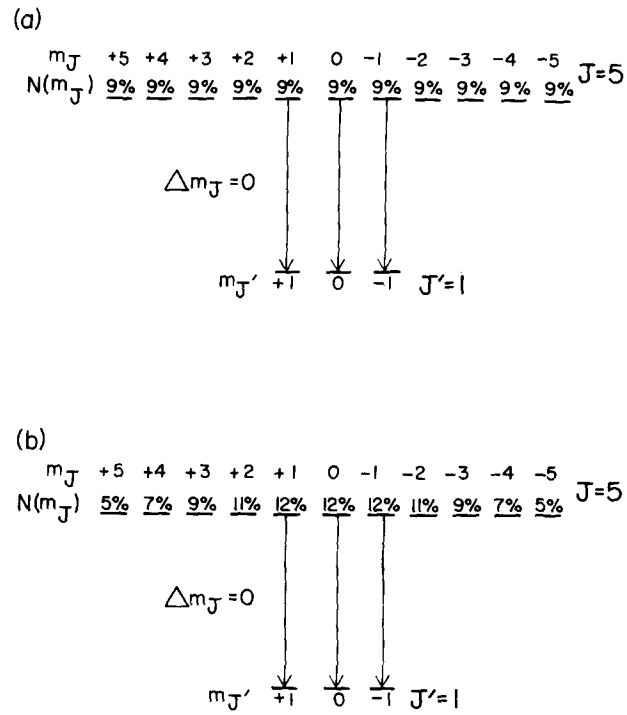

FIG. 15. Schematic diagram showing the influence of the m_J distribution of rotors on measured $R \leftrightarrow T$ cross sections. Assuming an m_J conserving selection rule for rotationally inelastic collisions, the top panel shows that 27% of the $J=5$ rotors are available for $R \rightarrow T$ transfer to $J'=1$ if the m_J distribution is random. The lower panel shows that this fraction increases for nonrandom m_J distributions produced by plane-polarized laser pumping or by supersonic expansion, both of which can preferentially populate low $|m_J|$ levels. The lower panel assumes a $\cos^2\theta$ distribution of molecular dipoles, as discussed in the text.

energy of 4 kcal/mol. The calculated downward cross section in this case is for the reverse of the transition $J=1$, $T_i=4$ kcal/mol $\rightarrow J'=5$, $T_f=2$ kcal/mol, which is the transition $J=5$, $T_i=2$ kcal/mol $\rightarrow J'=1$, $T_f=4$ kcal/mol. The measured downward cross section, however, is for a higher collision energy and correspondingly higher final translational energy; i.e., $J=5$, $T_i=4$ kcal/mol $\rightarrow J'=1$, $T_f=6$ kcal/mol. As the initial collision energy of the measured cross sections is increased, the energy transferred in $R \rightarrow T$ inelastic collisions becomes a smaller fraction of the initial translation energy. In the limit of high collision energy, the translation energy would not change significantly during $R \rightarrow T$ energy transfer. Thus, if the difference in translational energy were the source of the failure of the measured cross sections to satisfy degeneracy-averaged microscopic reversibility, the discrepancy should decrease upon increasing the initial collision energy of the measured cross sections. This is observed not to be the case as is evidenced by Table V; the indications are that the discrepancies may even increase slightly with collision energy.

The angular momentum degeneracies g_i and g_f are present in Eq. (6) to account for the difference in the number of degenerate exit channels available in upward and downward transitions. This assumes that m_J (the projection of the rotational angular momentum vector on the relative collision axis) is randomized during $R \rightarrow T$ inelastic collisions. In this case, all of the $m_{J'}$ levels in the final rotational state J' are accessible from any m_J level in the initial rotational state J. The cross section is then proportional to the degeneracy of the final state, namely $\sigma_{J \rightarrow J'} \propto (2J'+1)$. Consequently, the factor g_f/g_i in Eq. (6) is given by

$$\frac{\sigma_{J \rightarrow J'}}{\sigma_{J' \rightarrow J}} \propto \frac{(2J'+1)}{(2J+1)} .$$

However, the factor g_f/g_i may be modified if m_J is not randomized during $R \rightarrow T$ inelastic collision. As an example, if m_J is conserved during $R \rightarrow T$ inelastic collisions, i.e., $\Delta m_J = 0$, the number of degenerate exit channels is unity for both upward and downward transitions. However, in the case of downward transitions, transfer out of certain m_J levels would not be permitted. This is demonstrated in Fig. 15 for our exemplary transition $J=5 \rightarrow J'=1$. Only that fraction of the initial population which is in $m_J = 0, \pm 1$ is capable of contributing to the measured $J=5 \rightarrow J'=1$ cross section. If the initial m_J population distribution is random (i.e., equal population in all m_J levels), as illustrated in the top panel of Fig. 15, the fraction of the initial population which is available for the downward transition $J \rightarrow J'$ is only $(2J'+1)/(2J+1)$, while the measured upward cross sections would be independent of the angular momentum degeneracies. This dependence on J and J' may be expressed as

$$\sigma_{J \rightarrow J'} \propto \frac{(2J_< + 1)}{(2J+1)} , \tag{8}$$

where $J_<$ is the lesser of J and J'. It follows that the ratio of upward and downward cross sections is

$$\frac{\sigma_{J \rightarrow J'}}{\sigma_{J' \rightarrow J}} \propto \frac{(2J'+1)}{(2J+1)} . \tag{9}$$

This is identical to the ratio of Eq. (7), which was derived under the assumption of m_J randomization during $R \rightarrow T$ inelastic collisions. Thus, the assumption of a $\Delta m_J = 0$ selection rule, by itself, does not alter the relationship of upward and downward measured cross sections if the initial m_J distribution is random.

In the present study, the initial m_J distribution with respect to the relative collision axis may have been nonrandom. One probable cause of nonrandom m_J is the excitation of the initial rotational state by plane-polarized radiation from a cw chemical laser. The probability of excitation with plane polarized radiation is given classically by a $\cos^2\theta$ distribution, where θ is the angle between the transition dipole moment μ, which is perpendicular to the angular momentum vector of HF, and the electric vector of the exciting radiation ϵ. The electric vector of the laser radiation was oriented parallel to the HF molecular beam axis, and thus should have preferentially pumped HF molecules whose angular momentum vectors were perpendicular to the beam axis.

Since the relative velocity vector of the collision partners was dominated by the HF velocity vector (see Fig. 5), the molecular beam axis is approximately equivalent to the relative collision axis. Therefore, the laser exci-

tation should have preferentially pumped HF molecules with angular momentum vectors perpendicular to the relative collision axis. This would correspond to a nonrandom m_J distribution with an excess population in low $|m_J|$ levels.

Three effects which could in principle have resulted in a more nearly random m_J distribution in spite of the polarization of the exciting radiation are: (i) rotation of ϵ during the multiple reflections of the laser within the absorption cell; (ii) the distribution of relative velocity vectors; (iii) elastic collisions reorienting the angular momentum vector preceding rotationally inelastic encounters. The rotation of ϵ within the multiple pass cell was measured and found to be less than 15° after 24 reflections. The relative velocity vector was well defined due to the dominant contribution of the HF velocity vector which had an angular divergence of ±10°. Reorientation of the angular momentum vector during elastic collisions has been shown by close-coupling calculations to have a cross section of comparable magnitude to rotationally inelastic scattering.[45] Thus, it is unlikely that the above three considerations resulted in a randomized initial m_J distribution.

The m_J distribution which would result from laser excitation to the $J=5$ rotational state is shown in Fig. 15(b). As a consequence of such a nonrandom m_J distribution, a larger fraction of the initial population would be capable of making downward transitions under the restriction that $\Delta m_J = 0$. In the case of the $J=5 \rightarrow J'=1$ transition illustrated in Fig. 15(b), the percentage of the initial population which would be available for $R \rightarrow T$ transfer increased from 27% for a random m_J distribution (top panel of this figure), to 36% for the nonrandom m_J distribution (bottom panel). The ratio g_f/g_i in the expression for microscopic reversibility [Eq. (6)] would be 0.36 instead of $(2J'+1)/(2J+1) = 0.27$. The resulting increase in the downward cross section calculated by microscopic reversibility would however, only reduce the discrepancy (Table V) from 42% to 27%. Similar calculations involving the other transitions related by microscopic reversibility showed the same effect. Thus the assumption of a $\Delta m_J = 0$ selection a nonrandom initial m_J distribution operates in the right direction but is unable to account completely for the failure of the measured cross sections to satisfy microscopic reversibility.

As a check on the above considerations, an experiment was performed in which the electric vector of the exciting radiation was rotated by 90° from its usual orientation parallel to the molecular beam axis. By rotating the electric vector of the laser with respect to the molecular beam axis, any nonrandom initial m_J distribution due to laser pumping would be significantly altered in favor of higher $|m_J|$. The measured downward cross sections were thus expected to decrease relative to the upward cross sections. No experimentally significant change in the relative cross sections was observed, however.

A possible solution to this riddle is that it is the supersonic expansion of the HF, rather than the laser excitation, that is responsible for the major part of the alignment of rotation.[46] If our expansion were to produce an alignment consistent with a more sharply peaked distribution over m_J states than that indicated in the lower panel of Fig. 15 (about double the indicated proportion of molecules in $m_J = 0, \pm 1$) then application of the selection rule $\Delta m_J = 0$ to the upward and downward transitions would suffice to bring our results from the direct measurement into agreement with those calculated on the basis of microscopic reversibility.

It should be noted that the peculiarity discussed in this section is not an outgrowth of the application of the energy-gap expression, but stands independently of it. We also point out that this peculiarity may provide indirect evidence for an m_J conservation selection rule, heretofore reported only as a consequence of models used for interpreting $R \rightarrow T$ energy transfer.[47,48]

D. Quantum mechanical scaling relationship

An *a priori* scaling relationship between rotational inelastic cross sections has recently been derived and has allowed the extraction of dynamical state-to-state information from vibration–rotation linewidth data.[49] This scaling relationship has also been applied in the correlation and prediction of experimental state-to-state cross sections for $Na_2^* + Xe$.[47] Unlike the previously considered empirical relationships (see Sec. IV B above), the parameters for this scaling relationship have some dynamical significance.

The scaling relationship is derived within the quantal framework of the infinite-order sudden (IOS) approximation,[15,17] and is corrected to account for the molecular energy spacing and the finite collision duration. For rotationally inelastic collisions between an atom and a linear molecule, the expression obtained by means of the energy-corrected sudden (ECS) approximation is

$$\sigma_{J \rightarrow J'} = (2J'+1) \sum_{L=J-J'}^{J+J'} (2L+1) \begin{pmatrix} J & J' & L \\ 0 & 0 & 0 \end{pmatrix}^2 |A_L^J|^2 \sigma_{L \rightarrow 0}\,, \tag{10}$$

with the restriction that $J > J'$. Microscopic reversibility may be used to scale cross sections with $J < J'$. In the above expression, $(: : :)$ is a 3-j symbol accounting for the coupling of J and J' through L. The factor A_L^J, which is given in terms of an "effective collision length" l_c as

$$A_L^J = \frac{6 + [(\Delta E_{L,L-1}) l_c / 2v\hbar]^2}{6 + [(\Delta E_{J,J-1}) l_c / 2v\hbar]^2} \tag{11}$$

is termed an adiabaticity factor. It makes allowance for the finite collision time $\tau_c = l_c/v$; in the limit that $l_c \rightarrow 0$ or $\Delta E_{JJ'} \rightarrow 0$, $A_L^J = 1$ and Eq. (10) reduced to the IOS scaling expression.[15,17]

As a test of the ECS scaling relationship, the parameters l_c and $\sigma_{L \rightarrow 0}$ were varied in an iterative nonlinear fitting routine until the best fit to the experimental cross sections was obtained. A satisfactory fit to both upward and downward cross sections could not be obtained with a single set of fitting parameters. Instead, they were fit separately, and the parameters of the best fit to the $R \rightarrow T$ cross sections of HF + Ar at $T_i = 9$ kcal/mol are shown in Table VI. Also shown is a matrix of the calculated cross sections. The deviations from the mea-

TABLE VI. Cross section matrix for HF+Ar at $T_i = 9$ kcal/mol, calculated from the ECS scaling relationship [Eqs. (10) and (11)].

Final state	Initial State J				
J'	1	2	3	4	5
0	0.76	0.28	0.093	···	0.039
1		0.79	0.32	0.19	0.11
2	0.99		0.73	0.35	0.21
3	0.49	0.78		0.60	0.34
4	0.25	0.38	0.67		0.52
5	0.14	0.21	0.32	0.57	
6	0.060	0.11	0.17	0.26	0.48
7	0.067	0.055	0.095	0.142	0.22
8	0.057	0.059	0.050	0.082	0.121
9	0.052	0.052	0.054	···	0.071

Fitted parameter	$J' < J$	$J' < J$
l_c	8.6 Å	1.54 Å
$\sigma(1 \rightarrow 0)$	0.76	0.41
$\sigma(2 \rightarrow 0)$	0.28	0.14
$\sigma(3 \rightarrow 0)$	0.093	0.060
$\sigma(4 \rightarrow 0)$	0.047	0.021
$\sigma(5 \rightarrow 0)$	0.039	0.005

sured cross sections are generally within the statistical uncertainty of the data.

Since the relative cross sections, except for $\sigma_{1\rightarrow 0}$, were found to be independent of collision energy, the fitted parameters were independent of collision energy except for the effective collision length l_c which increased in proportion to the relative velocity. This trend is not significant, however, due to the insensitivity of the quality of the fit to l_c. The difference in l_c for upward and downward cross sections, 1.5 and 8.6 Å, respectively, is significant, however. This is in contrast to the only other such data, namely the state-to-state cross sections for $Na_2^* + Xe$ in which both upward and downward cross sections were fit by a single collision length of 3.7 Å.[47]

E. Dynamics

Except for the $J = 1 \rightarrow J' = 0$ transition, the relative $R \rightarrow T$ cross sections for HF + inert gas atoms measured in this work have been shown to be independent of HF vibration, center-of-mass collision energy and inert gas collision partner. These observations may be related to the anisotropy of the intermolecular potential which produces the torque necessary for $R \rightarrow T$ energy transfer.

Intermolecular potentials calculated by the electron gas model for HF + He and HF + Ar[50] do not differ greatly in the anisotropy of their repulsive walls, nor does the anisotropy in either case change greatly with the height on the repulsive wall. Figure 16 illustrates the invariance of the anisotropy of these potentials with height on the repulsive wall.[50] Also shown is the region probed by the maximum and minimum translational energies of the present study. In addition the anisotropy of the wall was found to be insensitive to an extension of the HF bond length from that corresponding to $v = 1$ to a value appropriate to $v = 2$.[51]

The observed independence of the majority of the $R \rightarrow T$ cross sections on the collision parameters studied (vibrational excitation, collision energy, and inert gas collision partner) appears to be consistent with the information that we have regarding the repulsive wall of the intermolecular potential. The dominant role of the repulsive wall in $R \rightarrow T$ inelastic scattering at enhanced collision energies has been noted previously in a classical trajectory study of HCl + Ar.[16]

By analogy to the trend in the intermolecular potentials of Ne + Ne, Ar, Kr,[52] the depth of the attractive well of the HF + Ne potential is expected to be markedly less than with either Ar or Kr as the collision partner. The small cross section for the $J = 1 \rightarrow J' = 0$ transition in HF + Ne as compared with the other inert gases is interpreted as being the result of a similar decrease in the depth of the attractive well in the intermolecular potential. The effectiveness of the attractive well in enhancing the $J = 1 \rightarrow J' = 0$ cross section would be expected to decrease with increasing collision energy. This is consistent with the observation of the diminishing $\sigma_{1\rightarrow 0}$ "anomaly" (the anomaly consisting in an unexpectedly high $\sigma_{1\rightarrow 0}$ relative to all other $R \rightarrow T$ σ's) as the collision energy is increased. The anomaly for HF + Ar decreases markedly as $T_i = 4$ is increased to $T_i = 9$ kcal/mol. The anomaly decreases to a measurable extent even in the range of collision energies $T_i = 9$ to $T_i = 16$ kcal/mol. This is noteworthy since the depth of the HF

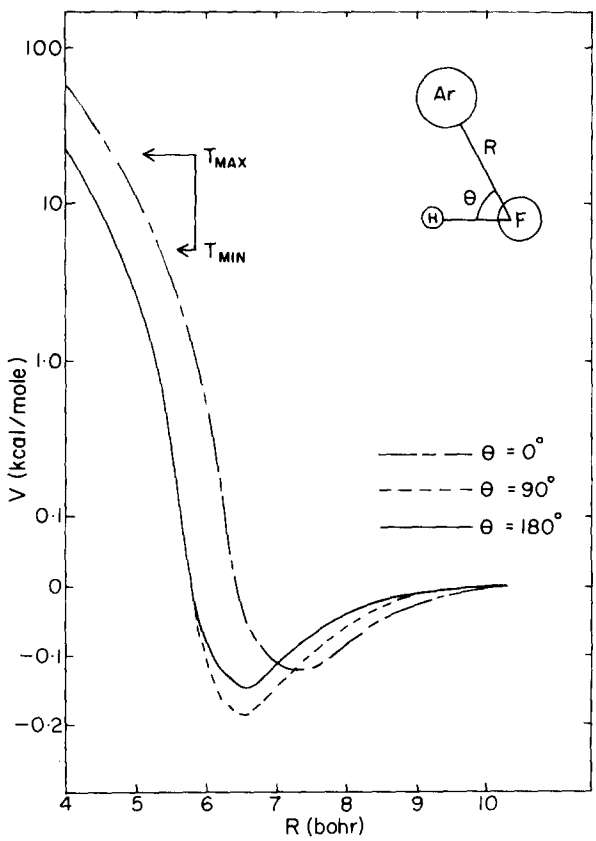

FIG. 16. Variation of the Ar–HF interaction energy with Ar to HF center-of-mass separation R and angle θ calculated by the electron–gas model, for HF at its $v = 0$ equilibrium separation. The curves were computed by Detrich and Conn (Ref. 50).

+ Ar potential well has been estimated to be ~ 0.35 kcal/mol[50]; it would appear that this well has a measurable effect on the anisotropy of interaction in large impact parameter collisions corresponding to the large $\sigma_{1\to 0}$, even at $T_t = 9$ kcal/mol.

Attractive interactions in He–Ar elastic scattering have been shown to have a significant effect in calculations of elastic cross sections at collision energies ~ 30 times the van der Waals attractive well depth.[53] The effectiveness of the attractive well in enhancing the elastic cross section has also been noted in a classical trajectory study of $R \rightarrow T$ in HCl + He, Ar.[16] The calculated $R \rightarrow T$ inelastic cross sections out of $J = 8$, by contrast, were shown to be insensitive to the potential well. The small amount of rotational energy, 0.1 kcal/mol, transferred in the $J = 1 \rightarrow J' = 0$ inelastic encounter between HF and inert gas makes it plausible that in this instance, as in elastic scattering, the potential well could have a significant effect on the cross section.

V. SUMMARY

(1) The exponential gap expression previously proposed for rotational-to-translational ($R \rightarrow T$) energy transfer in hydrogen halides[20] has been shown to significantly underestimate the cross sections for large transfers of energy in HF + rare gas $R \rightarrow T$ inelastic collisions. The HF $R \rightarrow T$ cross sections have been shown to scale as an inverse power of the energy transferred[9,54] which was as large as 55% of the energy available in translation.

(2) The exponent γ in the power gap expression was found to be independent of the initial J, initial translational energy, and the collision partner, but was dependent on the direction of energy transfer (i.e., $R \rightarrow T$ vs $T \rightarrow R$). The values of γ observed for HF + Rg atoms ($\gamma = 1.1$ for $R \rightarrow T$; $\gamma = 1.3$ for $T \rightarrow R$) were comparable to those of other experimental and theoretical systems treated in this fashion recently.[22] Though the apparent simplicity and universality of the power gap expression is appealing, the lack of a theoretical foundation at present precludes further developments in the theory.

(3) The $R \rightarrow T$ cross sections have also been shown to be consistent with a relationship based on the energy-corrected sudden approximation.[47] In contrast to the power-gap expression, this scaling relation has a theoretical foundation and the fitted parameters have some physical significance. It was necessary to fit upward and downward cross sections separately, the value of the effective collision length being 1.5 and 8.6 Å, respectively.

(4) The relative state-to-state cross sections were shown to be independent of the collision energy and the collision partner, except for the downward transition $J = 1 \rightarrow J' = 0$. The majority of the observed $R \rightarrow T$ inelastic scattering was interpreted as occurring on the repulsive wall of the intermolecular potential, which shows little change in anisotropy with collision energy.[50] However, $\sigma(1 \rightarrow 0)$ showed evidence of being sensitive to the shallow van der Waals attractive well.

(5) It was found that the measured cross sections for corresponding upward and downward transitions have rotational degeneracy factors consistent with a nonrandom distribution over the initial m_J states. This may provide evidence for partial conservation of the m_J quantum number for HF + Rg rotationally inelastic collisions. Systems with potential energy surfaces having their lowest minima in nonperpendicular orientations seem to conserve m_J during rotationally inelastic collisions.[55]

ACKNOWLEDGMENTS

The authors have benefited from discussions with Professor M. H. Alexander, Professor K. Bergmann, and Professor D. E. Pritchard, to whom they extend their thanks.

M.K. thanks the Killam Committee of the Canada Council for a Research Associateship. This work was supported by the Natural Sciences and Engineering Research Council (NSERC), to whom J.A.B. is additionally indebted for a scholarship.

[1] For recent reviews, see J. P. Toennies, Ann. Rev. Phys. Chem. **27**, 225 (1976); M. Faubel and J. P. Toennies, Adv. At. Mol. Phys. **13**, 229 (1977).
[2] H. E. van den Bergh, M. Faubel, and J. P. Toennies, Faraday Discuss. Chem. Soc. **55**, 203 (1973); M. Faubel and J. P. Toennies, J. Chem. Phys. **71**, 3770 (1979).
[3] H. Schmidt, V. Hermann, and F. Linden, Chem. Phys. Lett. **41**, 365 (1976).
[4] U. Buck, F. Huisken, J. Schleusener, and H. Pauly, Phys. Rev. Lett. **38**, 680 (1977); U. Buck, F. Huisken, and J. Schleusener, J. Chem. Phys. **68**, 5654 (1978).
[5] W. R. Gentry and C. F. Giese, J. Chem. Phys. **67**, 6380 (1977); W. R. Gentry and C. F. Giese, Phys. Rev. Lett. **39**, 1259 (1977).
[6] M. Faubel, K. H. Kohl, and J. P. Toennies, J. Chem. Phys. **73**, 2506 (1980).
[7] J. P. Toennies, Z. Phys. **182**, 257 (1965); V. Borkenhagen, H. Malthan, and J. P. Toennies, J. Chem. Phys. **71**, 1722 (1979).
[8] P. J. Dagdigian, B. E. Wilcomb, and M. H. Alexanfer, J. Chem. Phys. **71**, 1670 (1979); B. E. Wilcomb and P. J. Dagdigian, *ibid.* **67**, 3829 (1977).
[9] T. A. Brunner, R. D. Driver, N. Smith, and D. E. Pritchard, J. Chem. Phys. **70**, 4155 (1979); M. Wainger, I. Al-Agil, T. A. Brunner, A. W. Karp, N. Smith, and D. E. Pritchard, *ibid.* **71**, 1977 (1979).
[10] C. R. Vidal, Chem. Phys. **35**, 215 (1978).
[11] N. C. Lang, J. C. Polanyi, and J. Wanner, Chem. Phys. **24**, 219 (1977).
[12] J. J. Hinchen and R. H. Hobbs, J. Chem. Phys. **65**, 2732 (1976).
[13] (a) K. Bergmann, R. Engelhardt, U. Hefter, P. Hering, and J. Witt, Phys. Rev. Lett. **40**, 1446 (1978); (b) K. Bergmann, R. Engelhardt, U. Hefter, and J. Witt, J. Chem. Phys. **71**, 2726 (1979).
[14] (a) J. A. Serri, A. Morales, W. Moskowitz, D. E. Pritchard, C. H. Becker, and J. L. Kinsey, J. Chem. Phys. **72**, 6304 (1980); (b) J. A. Serri, C. H. Becker, M. B. Elbel, J. L. Kinsey, W. P. Moskowitz, and D. W. Pritchard, *ibid.* **74**, 5116 (1981).
[15] See, for example, R. Goldflam, D. J. Kouri, and S. Green, J. Chem. Phys. **67**, 5661 (1977), and references therein.
[16] (a) J. C. Polanyi, N. Sathyamurthy, and J. L. Schreiber, Chem. Phys. **29**, 105 (1977); (b) J. C. Polanyi and N. Sathyamurthy, *ibid.* **29**, 9 (1978), and references therein.
[17] See, for example, G. A. Parker and R. T Pack, J. Chem.

Phys. **68**, 1585 (1978), and references therein.
[18]A. E. De Pristo, S. D. Augustin, R. Ramaswamy, and H. Rabitz, J. Chem. Phys. **71**, 850 (1979).
[19]M. H. Alexander, J. Chem. Phys. **71**, 1683 (1979).
[20]J. C. Polanyi and K. B. Woodall, J. Chem. Phys. **56**, 1563 (1972).
[21](a) R. D. Levine, R. B. Bernstein, P. Kahana, I. Procaccia, and E. T. Upchurch, J. Chem. Phys. **64**, 796 (1976); (b) M. D. Pattengill and R. B. Bernstein, *ibid.* **65**, 4007 (1976).
[22]D. E. Pritchard, N. Smith, R. D. Driver, and T. A. Brunner, J. Chem. Phys. **70**, 2115 (1979).
[23]N. Smith, T. A. Brunner, A. W. Karp, and D. E. Pritchard, Phys. Rev. Lett. **43**, 693 (1979).
[24]R. E. Kutina, Ph. D. thesis, University of Toronto (1980).
[25]J. A. Barnes, M. Keil, R. E. Kutina, and J. C. Polanyi, J. Chem. Phys. **72**, 6306 (1980).
[26]A. M. G. Ding and J. C. Polanyi, Chem. Phys. **10**, 39 (1975).
[27]B. A. Esche, R. E. Kutina, N. C. Lang, J. C. Polanyi, and A. M. Rulis, Chem. Phys. **41**, 183 (1979).
[28]H. L. Welsh, C. Cumming, and E. J. Stansbury, J. Opt. Soc. Am. **41**, 712 (1951).
[29]J. B. Anderson, R. P. Andres, and J. B. Fenn, Adv. Chem. Phys. **10**, 275 (1966).
[30]J. Geddes, H. F. Krause, and W. L. Fite, J. Chem. Phys. **56**, 3298 (1972).
[31]J. J. Valentini, M. J. Coggiola, and Y. T. Lee, Rev. Sci. Instrum. **48**, 58 (1977).
[32]R. R. Stephens and T. A. Cool, Rev. Sci. Instrum. **42**, 1489 (1971).
[33]R. M. Osgood, Jr., P. B. Sackett, and A. Javan, J. Chem. Phys. **60**, 1464 (1974).
[34]B. A. Esche, M. Sc. thesis, University of Toronto (1975).
[25]R. O. Waddoups, *White Cells as Light Gatherers*, Scientific Report No. AFCRL-66-74, Department of Engineering, Utah State University (1966).
[36]R. N. Sileo and T. A. Cool, J. Chem. Phys. **65**, 117 (1976).
[37]P. E. Charters and J. C. Polanyi, Discuss. Faraday Soc. **33**, 107 (1962).
[38]U. Buck and P. McGuire, Chem. Phys. **16**, 101 (1976).
[39]L. Monchick and S. Green, J. Chem. Phys. **66**, 3085 (1977).
[40]C. H. Becker, P. W. Tiedemann, J. J. Valentini, and Y. T. Lee, J. Chem. Phys. **71**, 481 (1979).
[41]L. S. Blair, W. D. Breschears, and G. L. Schott, J. Chem. Phys. **59**, 1582 (1973).
[42]D. Brandt, L. W. Dickson, L. N. Y. Kwan, and J. C. Polanyi, Chem. Phys. **39**, 189 (1979).
[43]M. Rubinson and J. I. Steinfeld, Chem. Phys. **4**, 467 (1974).
[44]R. B. Bernstein, J. Chem. Phys. **62**, 4570 (1975).
[45]M. H. Alexander, Chem. Phys. **27**, 229 (1978).
[46]M. P. Sinha, C. D. Caldwell, and R. N. Zare, J. Chem. Phys. **61**, 491 (1974).
[47]R. Ramaswamy, A. E. DePristo, and H. Rabitz, Chem. Phys. Lett. **61**, 495 (1979).
[48]T. A. Brunner, N. Smith, and D. E. Pritchard, Chem. Phys. Lett. **71**, 358 (1980).
[49]A. E. DePristo and H. Rabitz, J. Chem. Phys. **69**, 902 (1978).
[50]J. Detrich and R. W. Conn, J. Chem. Phys. **64**, 3091 (1976).
[51]R. J. Fallon, J. T. Vanderslice, and E. A. Mason, J. Chem. Phys. **32**, 698 (1960).
[52]J. M. Parson, T. P. Schafer, F. P. Tully, P. E. Siska, Y. C. Wong, and Y. T. Lee, J. Chem. Phys. **55**, 5762 (1971).
[53]M. Keil and A. Kuppermann, J. Chem. Phys. **69**, 3917 (1978).
[54]B. C. Sanctuary, Chem. Phys. Lett. **62**, 378 (1979).
[55]M. Keil and H. R. Mayne, Chem. Phys. Lett. (in press).